© 2021. Published by The Company of Biologists Ltd | Development (2021) 148, dev199607. doi:10.1242/dev.199607

STEM CELLS AND REGENERATION

RESEARCH ARTICLE

Skeletal stem cell fate defects caused by *Pdgfrb* activating mutation

Hae Ryong Kwon[1], Jang H. Kim[1,2], John P. Woods[1,2] and Lorin E. Olson[1,2,*]

ABSTRACT

Autosomal dominant PDGFRβ gain-of-function mutations in mice and humans cause a spectrum of wasting and overgrowth disorders afflicting the skeleton and other connective tissues, but the cellular origin of these disorders remains unknown. We demonstrate that skeletal stem cells (SSCs) isolated from mice with a gain-of-function D849V point mutation in PDGFRβ exhibit colony formation defects that parallel the wasting or overgrowth phenotypes of the mice. Single-cell RNA transcriptomics with SSC-derived polyclonal colonies demonstrates alterations in osteogenic and chondrogenic precursors caused by PDGFRβ^{D849V}. Mutant cells undergo poor osteogenesis *in vitro* with increased expression of *Sox9* and other chondrogenic markers. Mice with PDGFRβ^{D849V} exhibit osteopenia. Increased STAT5 phosphorylation and overexpression of *Igf1* and *Socs2* in PDGFRβ^{D849V} cells suggests that overgrowth in mice involves PDGFRβ^{D849V} activating the STAT5-IGF1 axis locally in the skeleton. Our study establishes that PDGFRβ^{D849V} causes osteopenic skeletal phenotypes that are associated with intrinsic changes in SSCs, promoting chondrogenesis over osteogenesis.

KEY WORDS: Skeletal stem cells, Platelet-derived growth factor receptor beta, Penttinen syndrome, Kosaki overgrowth syndrome, Single-cell RNA-sequencing, Osteogenesis, Chondrogenesis, Osteopenia, Mouse

INTRODUCTION

Two platelet-derived growth factor receptors (PDGFRs) have been identified in mammals, PDGFRα and PDGFRβ, which bind to five PDGF ligands. PDGFRs play crucial and distinct roles in embryo development by regulating the proliferation, migration, survival and differentiation of many mesenchymal-derived cells that populate all tissues and organs (Andrae et al., 2008; Hoch and Soriano, 2003; Klinkhammer et al., 2018). It has recently been discovered that humans with gain-of-function mutations in *PDGFRB* exhibit a spectrum of phenotypes affecting the skeleton and other connective tissues in an autosomal-dominant fashion (Guérit et al., 2021). These mutations result in constitutive PDGFRβ signaling, causing Penttinen syndrome (MIM 601812) or Kosaki overgrowth syndrome (MIM 616592). Both disorders progressively affect the skeleton, beginning in childhood. Other activating variants of *PDGFRB* are associated with a milder phenotype, infantile myofibromas (MIM 228550), which does not affect the skeleton. Penttinen syndrome, with *PDGFRB* mutations V665A or N666S (mutated in the first kinase domain), is characterized as a premature aging condition with osteoporosis, scoliosis, lipoatrophy, dermal atrophy, aneurysms and acro-osteolysis (Bredrup et al., 2019; Johnston et al., 2015). Kosaki overgrowth syndrome, with *PDGFRB* mutations P584R or W566R (mutated in the juxtamembrane domain), is characterized by tall stature, elongated long bones, enlarged hands and feet, distinctive facial features, scoliosis, hyperelastic skin, aneurysms, myofibromas and neurodegeneration (Minatogawa et al., 2017; Takenouchi et al., 2015). The pathological mechanisms of the human disorders are still unknown.

We have previously demonstrated that mice with a gain-of-function D849V mutation in *Pdgfrb* (mutated in the second kinase domain, corresponding to the human D850 residue) died between 2-3 weeks of age after developing a postnatal wasting phenotype (He et al., 2017; Olson and Soriano, 2011). Surprisingly, these phenotypes were modulated by signal transducer and activator of transcription 1 (STAT1). Mice with *Pdgfrb*^{D849V} mutation but lacking *Stat1* (*Pdgfrb*$^{+/D849V}$*Stat1*$^{-/-}$ mice) survived until 8-9 weeks, becoming overweight and with widespread connective tissue overgrowth (not obesity), thick calvarias, abnormally curved spine and enlarged rib cage (He et al., 2017). Although the murine model clearly identified *Stat1* as a gene modulating the phenotype spectrum driven by *Pdgfrb*^{D849V}, many questions remain about the target cell types and signaling pathways underlying such striking phenotypes. Moreover, the role of PDGFRβ in the skeleton is not well understood, as PDGFRβ appears to be redundant for skeletal development based on the normal skeletal phenotypes of global and osteoblast-specific knockouts in mice (Bohm et al., 2019; Brun et al., 2020; Soriano, 1994).

Ligand binding to wild-type PDGFRβ induces receptor dimerization, which activates the kinase activity of the receptor and results in autophosphorylation of intracellular tyrosine residues that activate downstream signaling pathways (Lemmon and Schlessinger, 2010). Gain-of-function PDGFRβ mutations disrupt the inactive conformation of the receptor, leading to constitutive kinase activity and autophosphorylation. PDGFRs use a variety of signaling pathways to mediate their effects on cell behavior, including PI3K, MAPK, PLCγ and STAT1/3/5 (Demoulin and Essaghir, 2014; Heldin and Westermark, 1999; Tallquist and Kazlauskas, 2004). PDGFRβ is particularly important for pericyte development and function, but it is also expressed on fibroblasts, osteoblasts and stem/progenitor cells (Andrae et al., 2008).

Skeletal stem cells (SSCs) residing in bone and bone marrow (BM) are responsible for postnatal bone development, tissue homeostasis and repair (Bianco and Robey, 2015). A single SSC at the apex of skeletal lineages can give rise to chondrocytes, osteoblasts, adipocytes and fibroblasts. Recent findings with *in vivo* lineage tracing and single-cell transplantation have increased the

[1]Cardiovascular Biology Research Program, Oklahoma Medical Research Foundation, Oklahoma City, OK 73104, USA. [2]Department of Cell Biology, University of Oklahoma Health Sciences Center, Oklahoma City, OK 73104, USA.

*Author for correspondence (Lorin-Olson@omrf.org)

H.R.K., 0000-0002-0428-3971; L.E.O., 0000-0003-2168-7836

Handling Editor: Haruhiko Koseki
Received 12 March 2021; Accepted 28 October 2021

Development (2021) 148, dev199607. doi:10.1242/dev.199607

rigor of SSC biology and improved our understanding of SSC heterogeneity (Ambrosi et al., 2019; Serowoky et al., 2020). Perisinusoidal vasculature in BM is surrounded by SSCs expressing PDGFRβ, PDGFRα, CD146 [melanoma cell adhesion molecule (MCAM)], nestin (Nes), LepR and Cxcl12, whereas arterial vasculature is associated with SSCs expressing PDGFRβ, PDGFRα, stem cell antigen 1 (Sca1; also known as Ly6a) and LepR (Méndez-Ferrer et al., 2010; Morikawa et al., 2009; Sacchetti et al., 2007; Zhou et al., 2014). The resting zone of the growth plate harbors SSCs expressing Grem1, Col2a1, parathyroid hormone-related peptide (PTHrP; Pthlh) and Itgav (Chan et al., 2015; Mizuhashi et al., 2018; Newton et al., 2019; Worthley et al., 2015). The periosteum and cranial sutures contain SSCs expressing PDGFRβ, Gli1, Axin2, cathepsin K (Ctsk) and αSMA (Debnath et al., 2018; Ortinau et al., 2019; Shi et al., 2017; Yang et al., 2013; Zhao et al., 2015). PDGFRβ is broadly expressed in SSCs, but its role has not been examined. We speculated that PDGFRβ signaling could be functional in SSCs, and hypothesized that elevated *Pdgfrb*^{D849V} mutant signaling in SSCs could alter stem cell functions to generate skeletal disorders.

RESULTS

PDGFRβ^{D849V} alters skeletal growth in mice

To explore the PDGFRβ^{D849V} skeleton, we generated a cohort of mice and measured their weights and bone lengths. As *Stat1* is an important modifier of PDGFRβ^{D849V} phenotypes (He et al., 2017), four offspring genotypes were established with the *Sox2-Cre* driver for germline activation of *Pdgfrb*^{D849V} and/or deletion of *Stat1*-floxed alleles by crossing *Pdgfrb*$^{+/[s]D849V}$*Stat1*$^{flox/flox}$ and *Stat1*$^{+/-}$*Sox2-Cre*$^{+/-}$ mice. The resulting four genotypes are: *Stat1*$^{+/-}$ (hereafter designated as $S^{+/-}$), *Stat1*$^{-/-}$ ($S^{-/-}$), *Pdgfrb*$^{+/D849V}$*Stat1*$^{+/-}$ ($KS^{+/-}$), and *Pdgfrb*$^{+/D849V}$*Stat1*$^{-/-}$ ($KS^{-/-}$) (Fig. 1A). The *Pdgfrb* allele expressing D849V is designated K because the mutation is in the kinase domain. We used two genetic controls, $S^{+/-}$ and $S^{-/-}$, that do not show growth or survival defects (He et al., 2017; Meraz et al., 1996). $KS^{+/-}$ mice died by 3 weeks of age with features of autoinflammation and wasting. $KS^{-/-}$ mice, however, were rescued in survival at 3 weeks and died at around 8-9 weeks, consistent with previous findings (He et al., 2017). Thus, body weights were collected from live mice at 2-9 weeks of age, and bone length data were collected from tibias at 3 or 6-8 weeks of age. In the resulting growth curve, $KS^{+/-}$ and $KS^{-/-}$ mice were clearly

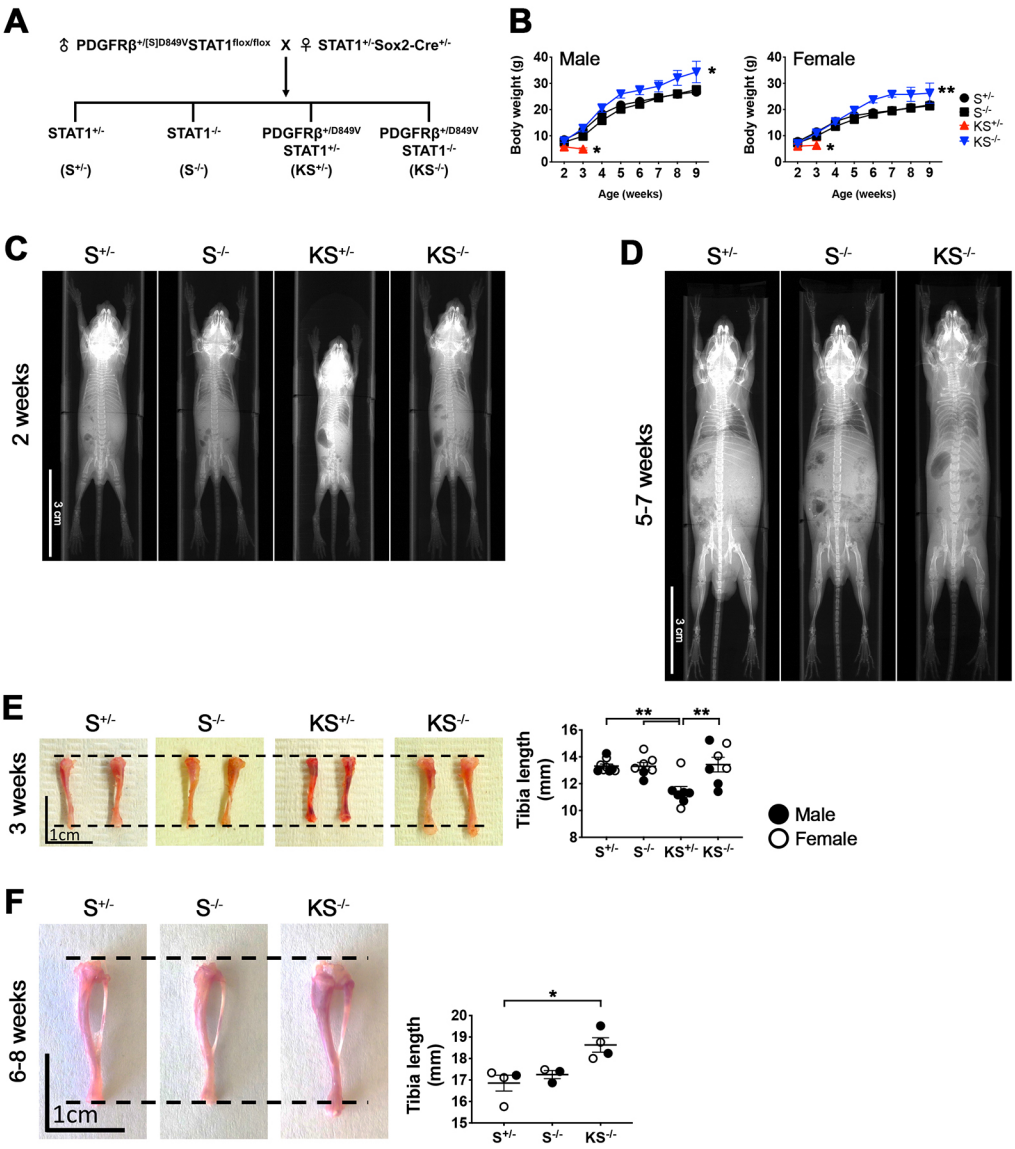

Fig. 1. PDGFRβ^{D849V} alters skeletal growth in mice. (A) The breeding scheme for generating four genotypes of offspring with germline activation of *Pdgfrb*^{D849V} and deletion of *Stat1*. *Pdgfrb*$^{+/[s]D849V}$ is a flox-stop-flox-*Pdgfrb*^{D849V} knock-in construct. *Sox2-Cre* is active in the female germline. (B) Male and female body weights of 2- to 9-week-old mice (males: *n*=5 for $S^{+/-}$, 8 for $S^{-/-}$, 3 for $KS^{+/-}$ and 10 for $KS^{-/-}$; females: *n*=8 for $S^{+/-}$ and $S^{-/-}$, 3 for $KS^{+/-}$ and 10 for $KS^{-/-}$). **P*<0.05, ***P*<0.01 $KS^{-/-}$ versus $S^{-/-}$ for 2- to 9-week-old females. **P*<0.05 $KS^{-/-}$ versus $S^{-/-}$ for 2- to 9-week-old males or $KS^{+/-}$ versus $KS^{-/-}$ for 2- to 3-week-old males and females. (C) Whole-body X-ray scan at 2 weeks of age (*n*=3 of each genotype). Representative images include 2-week-old male $S^{+/-}$ and female $S^{-/-}$, $KS^{+/-}$ and $KS^{-/-}$. (D) Whole-body X-ray scan at 5-7 weeks of age (*n*=3 of each genotype). Representative images include 5-week-old male $S^{+/-}$, 7-week-old female $S^{-/-}$ and 5-week-old male $KS^{-/-}$. (E) Tibia length measurements at 3 weeks old (*n*=9 for $S^{+/-}$ and 7 for $S^{-/-}$, $KS^{+/-}$ and $KS^{-/-}$). (F) Tibia length measurements at 6-8 weeks old (*n*=4 for $S^{+/-}$, 3 for $S^{-/-}$ and 4 for $KS^{-/-}$). Male and female data plotted with black and white circles, respectively. **P*<0.05, ***P*<0.01. Statistical analysis by two-way ANOVA (B) or one-way ANOVA (C,D). Data represent mean±s.e.m.

Development (2021) 148, dev199607. doi:10.1242/dev.199607

distinguishable by their obvious wasting and overgrowth phenotypes, respectively (Fig. 1B). Whole-body X-ray showed smaller bones in $KS^{+/-}$ at 2 weeks of age (Fig. 1C) and larger bones in $KS^{-/-}$ at 5-7 weeks of age (Fig. 1D) with an abnormally curved spine, as previously reported (He et al., 2017). Dissected 3-week-old $KS^{+/-}$ tibias were shorter than $KS^{-/-}$ and control tibias (Fig. 1E), and by 6-8 weeks the $KS^{-/-}$ tibias were significantly longer than controls (Fig. 1F).

PDGFRβ^{D849V} regulates PαS SSC numbers and colony formation

To determine whether SSCs were altered in PDGFRβ^{D849V}-expressing mice, we performed SSC quantification and colony formation assays. SSCs were immunophenotyped from limb bones with enzymatic digestion and flow cytometry using two well-established SSC markers, PDGFRα and Sca1 (PαS) (Houlihan et al., 2012; Morikawa et al., 2009) (Fig. S1A). The percentage of PαS SSCs in the stromal fraction (excluding hematopoietic and endothelial cells) was calculated at 3 and 6 weeks of age. The PαS percentage was similar between all genotypes at 3 weeks old (Fig. 2A), but it was significantly increased in cells isolated from $KS^{-/-}$ bones at 6 weeks old (Fig. 2B). To characterize stem cell function, we sorted PαS SSCs from 3-week-old and 6- to 9-week-old bones and performed colony formation assays. PαS SSCs showed an approximately ninefold increase in colony formation compared with freshly isolated whole bone marrow (WBM) (Fig. 2C). At 3 weeks there was a decrease in the number of colonies generated by $KS^{+/-}$ PαS SSCs compared with $S^{+/-}$ or $S^{-/-}$ cells, whereas the number of colonies was increased in $KS^{-/-}$ cells (Fig. 2D,E). The colonies were classified into groups based on size (small, <5 mm^2; medium, 5 mm^2<x<36 mm^2; large, >36 mm^2) to examine the expansion capacity of control and mutant SSCs. $KS^{+/-}$ SSCs generated decreased colony numbers of all three sizes, and $KS^{-/-}$ increased medium size colonies (Fig. 2E). Also, 6- to 9-week-old $KS^{-/-}$ SSCs increased the number of colonies formed compared with controls (Fig. 2F,G). Western blotting confirmed constitutive activation of PDGFRβ and knockout of STAT1 in SSC-derived cells (Fig. 2H). These results show that mice with PDGFRβ^{D849V} exhibit changes in the number of PαS SSCs and colony forming unit activity in parallel to the wasting and overgrowth phenotypes displayed *in vivo*, consistent with the idea of intrinsic defects in mutant SSCs mediating skeletal phenotypes.

Single-cell RNA-sequencing indicates multi-lineage potential of PαS SSC-derived cells

PαS-derived cells can differentiate into osteoblasts or adipocytes when treated with differentiation cocktails (Morikawa et al., 2009). However, we noted that our colonies were only partially differentiated (Fig. S1B,C), suggesting cellular heterogeneity within each colony. As an approach to evaluate cellular heterogeneity in SSC-derived polyclonal colonies, we performed single-cell RNA-sequencing (scRNA-seq). In principle, freshly isolated PαS SSCs would be attractive for scRNA-seq, but the $KS^{+/-}$ mutant mice suffer from systemic autoinflammation that inhibits colony formation (Fig. 2D,E) and would strongly influence gene expression. To escape this condition, we used SSC-derived colonies that had been cultured for 14 days in maintenance medium instead of freshly isolated cells. Single-cell suspensions of colony-forming units-fibroblasts

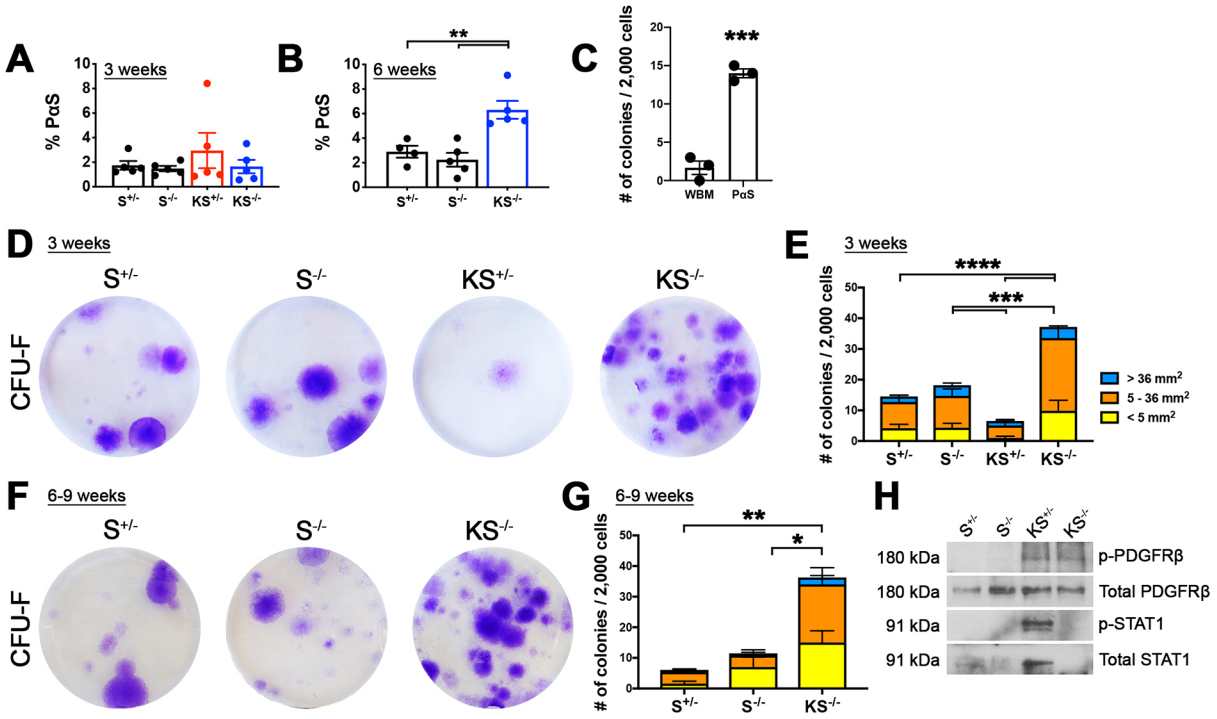

Fig. 2. PDGFRβ^{D849V} alters PαS SSC numbers and colony formation capacity. (A) Ratio of PαS SSCs in the stromal fraction (non-hematopoietic and non-endothelial skeletal pool) of compact bone from 3-week-old mice (n=5 for all four genotypes). (B) PαS SSCs ratio at 6 weeks old (n=4 for $S^{+/-}$ and 5 for $S^{-/-}$ and $KS^{-/-}$). (C) CFU-F rate of 2000 whole bone marrow (WBM) cells compared with 2000 PαS cells. (D-G) CFU-F colonies stained with Crystal Violet and quantified. PαS SSCs were isolated by FACS from 3-week-old (D,E) or 6- to 9-week-old (F,G) mice. CFU-F assays were performed with 2000 PαS SSCs isolated from individual mice in a 6-well plate. Quantification plots (E,G) show total colony numbers and three categories of colony size (n=6 mice for $S^{+/-}$, $S^{-/-}$ and $KS^{-/-}$ and 4 for $KS^{+/-}$ for 3 weeks, n=5 for $S^{+/-}$ and $S^{-/-}$ and 4 for $KS^{-/-}$ for 6-9 weeks). (H) Phosphorylated PDGFRβ (pY1009), total PDGFRβ, phosphorylated STAT1 (pY701) and total STAT1 in SSCs after overnight serum-starvation, representative of two biological replicates. Statistical analyses of E and G were performed with total numbers of colonies between genotypes. ****P<0.001, ***P<0.005, **P<0.01 and *P<0.05 by one-way ANOVA (A,B,E,G) and unpaired, two-tailed t-test (C). Data represent mean±s.e.m.

Development (2021) 148, dev199607. doi:10.1242/dev.199607

(CFU-Fs) from the four genotypes were subjected to scRNA-seq using 10x Genomics Chromium platform. We integrated scRNA-seq data from eight samples, representing the four genotypes in duplicate, to generate clusters using the Seurat package (Butler et al., 2018; Stuart et al., 2019). Data integration with canonical correlation analysis (CCA) removed batch effects (Fig. S2A). Each cluster was grouped based on signature genes that were differentially expressed between clusters (Fig. 3A). A heatmap of signature gene expression is shown in Fig. 3B (full list in Table S1). These markers, combined with current literature and gene ontology, were used to suggest cell types or cell fates represented by each cluster (Fig. 3C,D; Table S2). Clusters of biological duplicates were distributed similarly within each genotype (Fig. S2B). As shown by uniform manifold approximation and projection (UMAP) plot (Fig. 3A), we found ten clusters tentatively containing SSCs, intermediate skeletal stem and progenitor cells (SSPCs), chondrocyte precursors, osteoblast precursors or adipocyte precursors. All ten clusters were conserved across the four genotypes (Fig. S2C). These cell-type designations may represent potential cell fates rather than fully differentiated cell types. Our interpretations are based on current biological and gene ontology knowledge, but have not been functionally validated to determine their characteristics *in vivo*.

As a percentage of all cells, SSCs and SSPCs were more abundant than precursors (Fig. 3E). The most abundant was cluster 0 (26.6%, SSPCs with *Pdgfra*^{high}), followed by cluster 1 (21.9%, SSPCs with *Sca1*^{high}) and cluster 2 (11.1%, SSCs with *Pdgfra*^{high} and *Sca1*^{high}). Given the initial seeding of PαS SSCs, cluster 2 should be related to the origin of other clusters owing to high expression of *Pdgfra* and

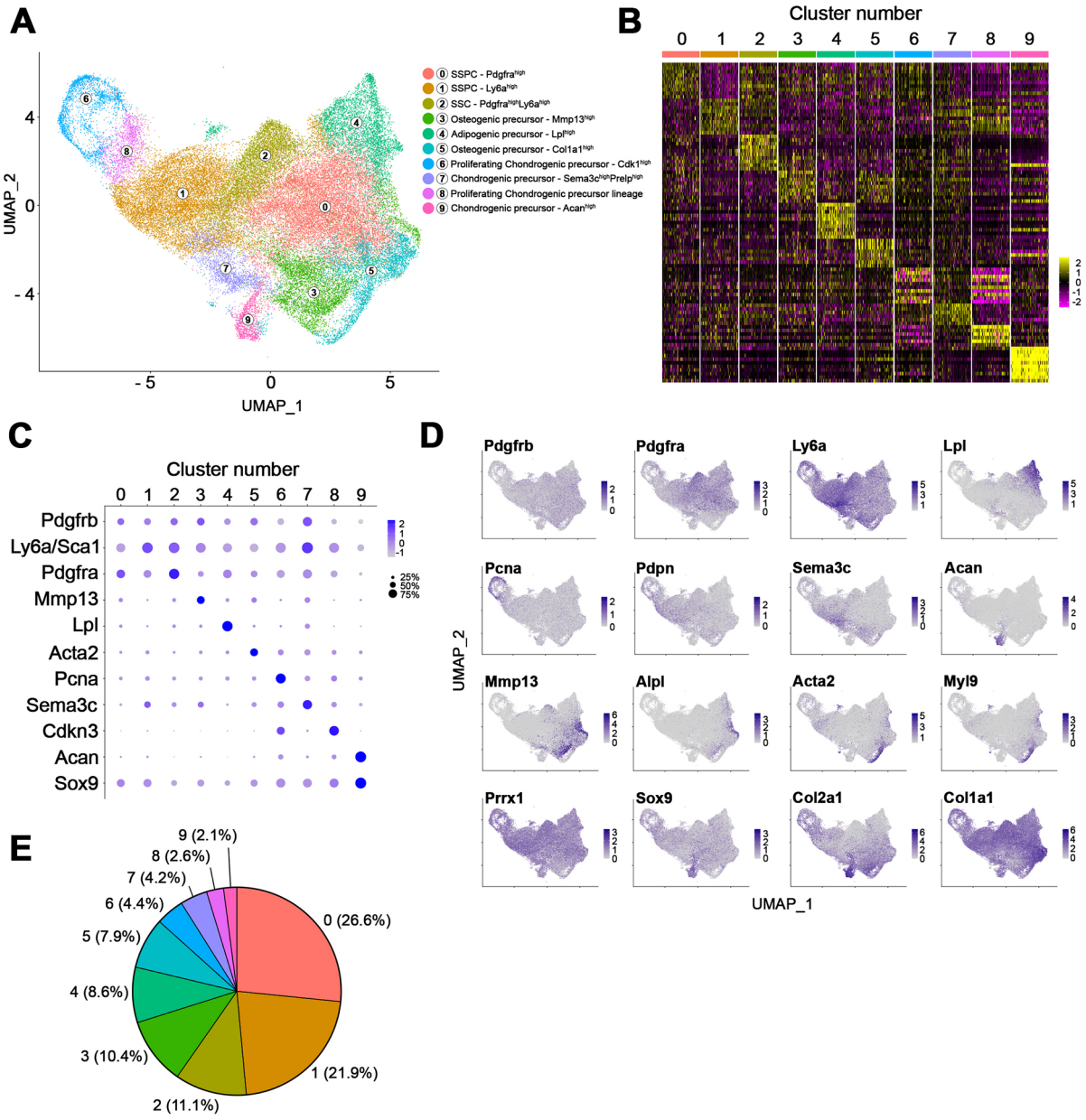

Fig. 3. scRNA-seq indicates multilineage potential of PαS SSC-derived cells. (A) UMAP plot showing ten clusters and their cell types. scRNA data from all four genotypes with biological duplicates were integrated and clustered by Seurat. (B) Heatmap generated with markers of ten clusters (see Table S1 for full list). (C) Dot plot of highly expressed markers in each cluster. Dot color indicates expression level and dot size indicates percentage of cells. (D) UMAP plot highlighting distribution of 16 markers. (E) Proportion of each cluster in the total population.

Development (2021) 148, dev199607. doi:10.1242/dev.199607

Sca1. The mesoderm transcription factor *Prrx1* was most highly expressed in cluster 2 and was broadly expressed in other clusters, as expected for SSCs and their progeny (Fig. S2D). *Pdgfrb* was moderately expressed in most clusters including SSCs (cluster 2), but was downregulated in chondrocyte precursors (clusters 6, 8 and 9) (Fig. 3C). The SSC and SSPC clusters broadly expressed several previously identified stem cell markers including *Cxcl12*, *Ctsk*, *Cd164*, *Itgav*, podoplanin (*Pdpn*) and *Grem1*, but others were barely detected including *Nes*, *Cd146* and *Lepr* (Fig. S2D). Previously, Nes-CreER^{+} BM cells were not enriched in CFU-Fs, suggesting that *Nes* expression should not be detectable in CFU-F (Zhou et al., 2014). Similarly, CD146 was found not to be an SSC marker on murine BM stromal cells (Chou et al., 2012). As mouse BM stromal cells begin to express *Lepr* after 3 weeks of age (Zhou et al., 2014), the absence of *Lepr* in our data is probably due to collecting PαS SSCs from 2- to 3-week-old mice.

The remaining clusters, 3 through 9, could be precursors rather than differentiated cells, because the cells were cultured under conditions to support clonal expansion without differentiation. Representative markers for each precursor cluster are summarized in Fig. S2E. Provisionally, cluster 3 represents osteogenic precursors expressing metalloproteinase 13 (*Mmp13*), alkaline phosphatase (*Alpl*) and osterix (*Sp7*). Cluster 4 represents adipocyte precursors expressing lipoprotein lipase (*Lpl*), fatty acid-binding protein 4 (*Fabp4*), haptoglobin (*Hp*) and adiponectin (*Adipoq*). Cluster 5 represents osteoblastic precursors highly expressing collagens *Col1a1* and *Col1a2* and moderately expressing actin alpha 2 (*Acta2*), transgelin (*Tagln*) and myosin light chain 9 (*Myl9*). Clusters 6 and 8 represent actively proliferating chondrocyte precursors highly expressing cell cycle genes (*Cdk1*, *Mki67* and *Pcna*) and early chondrogenic markers (*Col2a1* and *Grem1*). As we regressed out cell cycle genes (S and G2/M phase genes) during dimensional reduction of scRNA data, many S phase cells were distributed throughout all the clusters (Fig. S2F). However, clusters 6 and 8 remained prominent for cell cycle, chromosome and mitosis gene signatures (Table S2). Cluster 7 represents chondrogenic precursors with expression of semaphorin 3c (*Sema3c*) and proline arginine-rich end leucine-rich repeat protein (*Prelp*). Cluster 9 represents chondrocyte precursors with expression of aggrecan (*Acan*), unique cartilage matrix-associated protein (*Ucma*), collagens *Col9a1* and *Col2a1*, and the crucial chondrogenic transcription factor *Sox9* (Akiyama et al., 2002). Taken together, scRNA transcriptomics reveals the heterogeneity and potential cell fate transition of PαS SSC-derived cells.

Altered numbers of osteogenic and chondrogenic clusters associated with PDGFRβ^{D849V}

To identify changes in cell clusters and gene expression due to PDGFRβ^{D849V}, we compared scRNA data of four genotypes representing $S^{+/-}$, $S^{-/-}$, $KS^{+/-}$ and $KS^{-/-}$. *Pdgfrb* mRNA was moderately decreased in $KS^{+/-}$ and $KS^{-/-}$ genotypes, as shown previously in dermal fibroblasts (He et al., 2017), and *Stat1* mRNA was absent from $S^{-/-}$ and $KS^{-/-}$ (Fig. 4A). We compared the proportion of each cluster within the total population of each genotype and found subtle shifts in osteogenic and chondrogenic precursors. The proportional ratio of osteogenic clusters (clusters 3 and 5) was decreased in both mutants $KS^{+/-}$ and $KS^{-/-}$ compared with $S^{+/-}$ and $S^{-/-}$ controls (Fig. 4B,C; Table S6). This suggests that PDGFRβ^{D849V} signaling could suppress osteogenesis independently of *Stat1* status. Meanwhile, proliferating chondrocytes (clusters 6 and 8) and *Acan*^{high}-chondrogenic precursors (cluster 9) were increased in $KS^{+/-}$ compared with all other genotypes (Fig. 4B,C). $KS^{-/-}$ only slightly increased the proliferating chondrogenic precursors (cluster 8), but less than $KS^{+/-}$. This suggests PDGFRβ^{D849V}-mediated chondrogenic defects, potentially modulated by *Stat1* status.

PDGFRβ^{D849V} impairs osteogenesis and mineralization

To identify gene expression changes in osteogenic clusters, we analyzed scRNA data with the Database for Annotation, Visualization and Integrated Discovery (DAVID) analysis (Huang et al., 2009) (Tables S3,S4). We found that $KS^{+/-}$ and $KS^{-/-}$ cells downregulated osteogenesis-related genes including *Mmp13*, *Col1a1*, *Col1a2*, pentraxin 3 (*Ptx3*), plasminogen activator inhibitor-1 (*Serpine1*) and pigment epithelium-derived factor (*Serpinf1*) (Fig. 4D). Their expression levels were decreased in almost all $KS^{+/-}$ and $KS^{-/-}$ clusters, suggesting a broad impact across skeletal lineages (Fig. 4E). To examine osteogenic differentiation *in vitro*, we isolated heterogeneous skeletal cells from 3-week-old compact bone (see Materials and Methods). These cells include SSCs, SSPCs and progenitors with osteoblast potential. After culturing them with a standard cocktail of osteoblast differentiation inducers, $KS^{+/-}$ and $KS^{-/-}$ cells showed significantly reduced alkaline phosphatase (ALP) staining, consistent with defective osteoblast differentiation (Fig. 4F), and significantly reduced Alizarin Red (AR) staining, suggesting defective mineralization (Fig. 4G).

Next, to examine bone mass and mineralization in mice, we used micro computed tomography (microCT) to examine 3-week-old tibias from the four genotypes. $KS^{+/-}$ tibias decreased bone volume to total volume (BV/TV) and decreased bone mineral density (mg HA/ccm) in the cortical bone of the diaphysis (Fig. 5A) and the proximal tibial metaphysis (Fig. 5B) compared with $S^{+/-}$ and $S^{-/-}$ tibias. $KS^{+/-}$ microCT scans also displayed osteoporosis-like pores in the cortical bone (Fig. 5A). $KS^{+/-}$ tibias decreased trabecular thickness, but not trabecular number and separation (Fig. 5B). In contrast, $KS^{-/-}$ tibias at 3 weeks had no pores and partially normalized BV/TV and bone mineral density in both cortical and trabecular regions (Fig. 5A,B). There were no changes in trabecular number, thickness and separation in $KS^{-/-}$ compared with $S^{+/-}$ and $S^{-/-}$. However, 5- to 8-week-old $KS^{-/-}$ tibias displayed reduced BV/TV and bone mineral density in the cortical bone of the diaphysis (Fig. 5C) and the proximal tibial metaphysis (Fig. 5D) compared with age-matched $S^{+/-}$ and $S^{-/-}$ tibias. Trabecular numbers and thickness were decreased, but separation was increased in $KS^{-/-}$. We performed Calcein double staining to quantify mineral appositional growth rate (MAR). Histomorphometric analysis of cortical bone at 3 weeks showed decreased bone growth in $KS^{+/-}$, which was normalized in $KS^{-/-}$ (Fig. 5E). Interestingly, 6-week-old $KS^{-/-}$ cortical bone showed increased MAR compared with controls (Fig. 5F), but the Calcein labeling was thicker and more diffuse, which is consistent with incomplete or delayed mineralization. In summary, as suggested by transcriptomics, we found that PDGFRβ^{D849V} impairs osteogenesis and leads to osteopenia that becomes severe early in $KS^{+/-}$ mice (by 3 weeks) and later in $KS^{-/-}$ mice (by 6 weeks).

PDGFRβ^{D849V} and STAT1 augment chondrogenesis

The growth and survival phenotypes (Fig. 1B), and the time required to develop osteopenic phenotypes (Fig. 5), are very different between $KS^{+/-}$ and $KS^{-/-}$ mice. Furthermore, in SSC-derived polyclonal colonies, $KS^{+/-}$ prominently increased chondrogenic clusters (clusters 1, 6, 8 and 9) (Fig. 4B,C) including Sox9^{high} chondrogenic precursors (cluster 9) compared

Development (2021) 148, dev199607. doi:10.1242/dev.199607

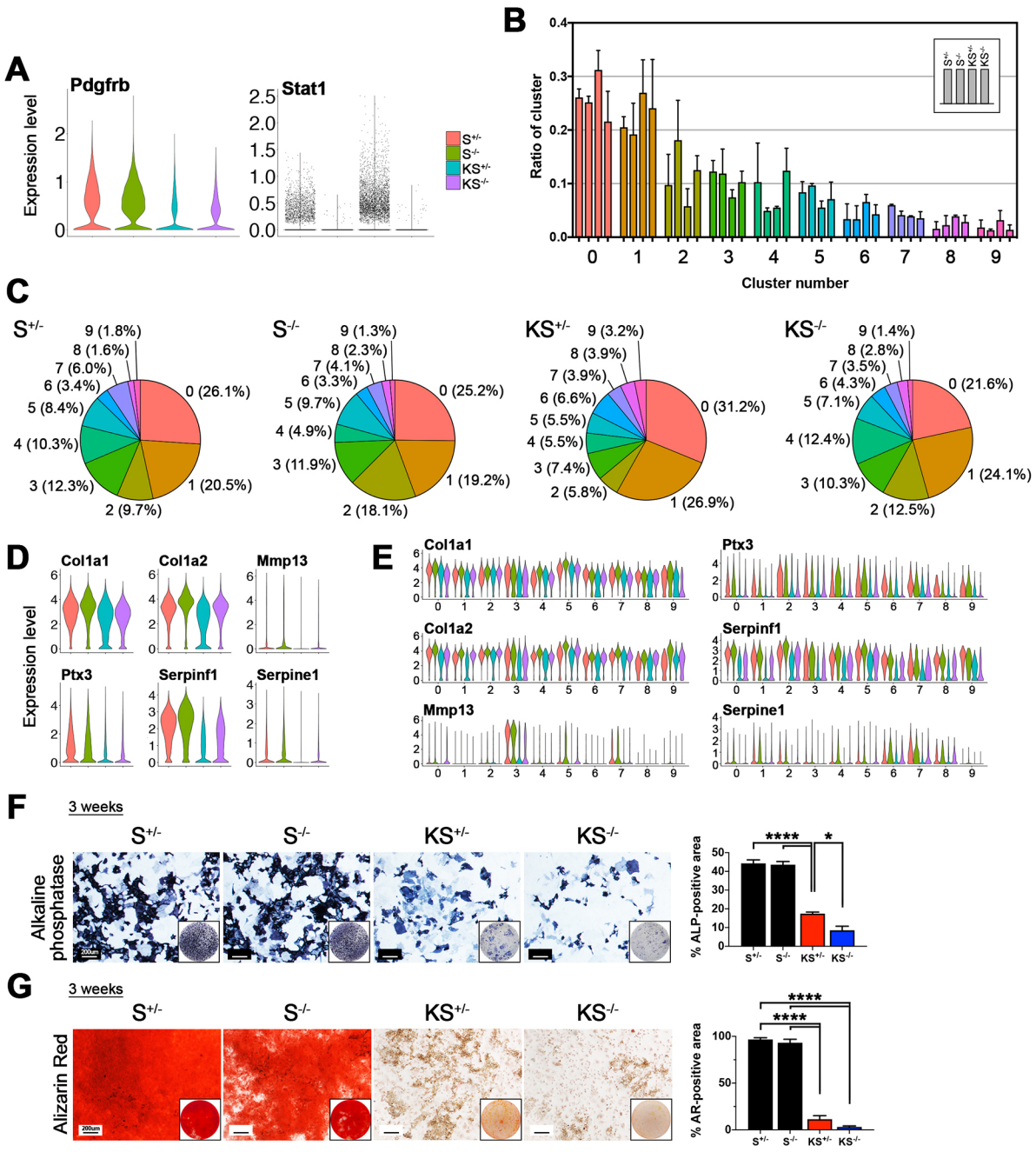

Fig. 4. Altered osteogenic capacity associated with PDGFRβ^{D849V}. (A) scRNA-seq subgrouped by four genotypes, showing expression levels of *Pdgfrb* and *Stat1*. (B) Proportional ratio of each cluster across four genotypes as bar graphs. (C) Proportional ratio of each cluster across four genotypes as pie charts with ratios labeled. (D) Violin plots showing expression of six significantly downregulated osteogenesis-related genes (*Col1a1*, *Col1a2*, *Mmp13*, *Ptx3*, *Serpinf1* and *Serpine1*) in mutant colonies. (E) Violin plots showing expression of the six genes shown in D across ten clusters in each genotype. (F) Primary skeletal cells stained for ALP after 2 weeks of osteoblast differentiation (n=3 biological replicates per genotype). (G) Primary skeletal cells stained with Alizarin Red after 4 weeks of osteoblast differentiation (n=3 biological replicates per genotype). ****P<0.001 and *P<0.05 by one-way ANOVA. Data represent mean±s.e.m.

with others (Fig. 6A). We further analyzed differentially expressed genes (DEGs) specific to the $KS^{+/-}$ genotype (Tables S3,S4). Among 34 genes specifically upregulated in $KS^{+/-}$ versus the other three genotypes, cartilage development genes were highly enriched, including *Sox9*, *Col2a1*, H19, imprinted maternally expressed transcript (*H19*) and *Acan* (Fig. 6B). Increased *Sox9*, *Col2a1* and *H19* expression was not limited to cluster 9, but also showed increased expression in other clusters (Fig. 6C; Fig. S3A). *Col2a1* and *H19* are known downstream targets of Sox9, which directly regulates collagen 2 production (Bell et al., 1997). Sox9 also indirectly promotes collagen 2 expression via a long non-coding RNA *H19* and its micro-RNA, *miR675* (Dudek et al., 2010). This suggests that increased Sox9 in $KS^{+/-}$ SSCs promotes chondrogenic proliferation and commitment. To evaluate chondrogenesis *in vivo*, we analyzed Safranin-O-stained tibias at 3 weeks old. $KS^{+/-}$ exhibited greater cartilage area in the tibia head, although $KS^{-/-}$ also showed mildly increased cartilage area (Fig. 6D). Note that $KS^{+/-}$ tibias were significantly smaller in size (Fig. 1C), and therefore the proportional area of $KS^{+/-}$ cartilage is much larger than the three other genotypes. We evaluated Sox9 expression *in vivo* in

Development (2021) 148, dev199607. doi:10.1242/dev.199607

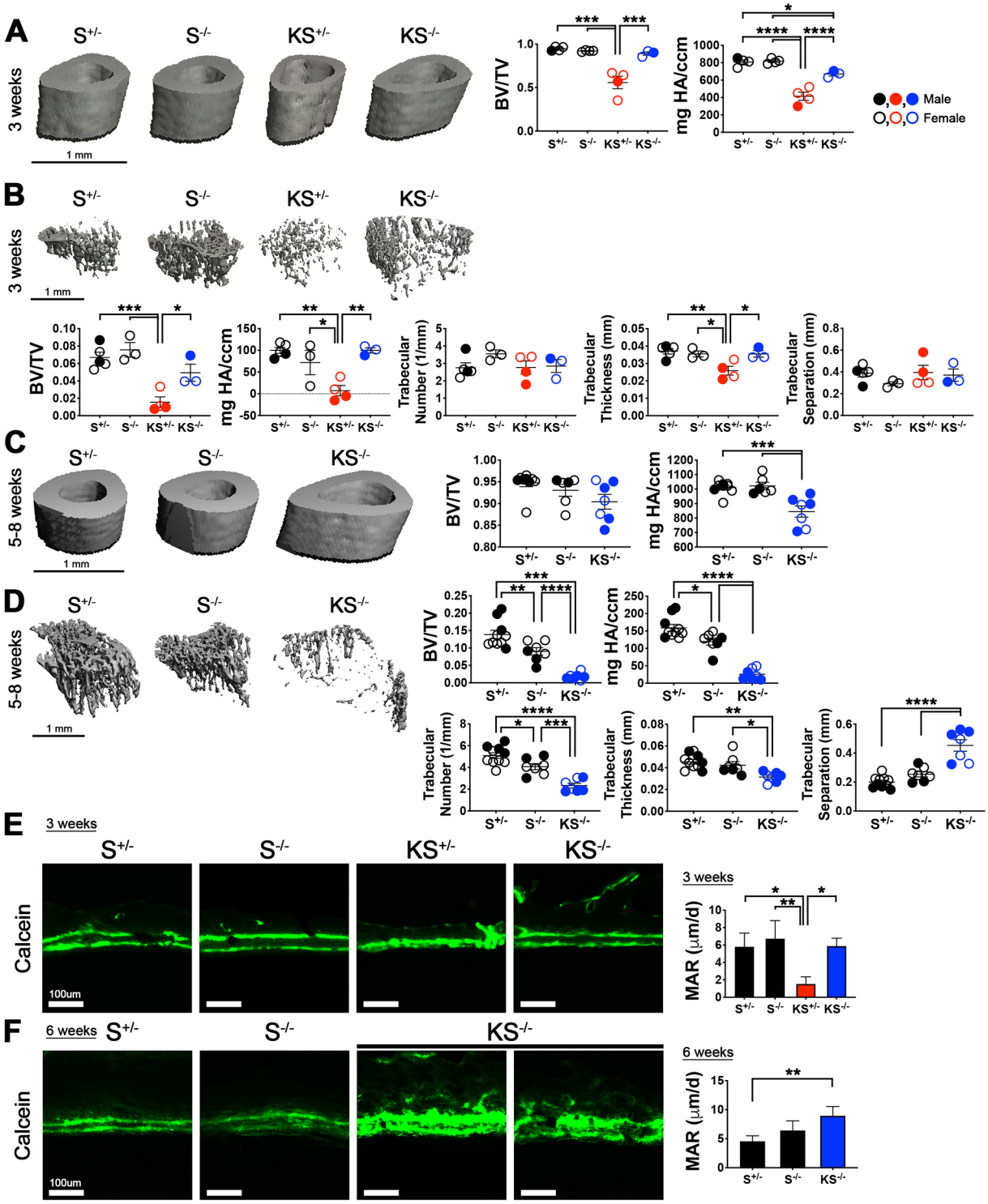

Fig. 5. PDGFRβ^{D849V} inhibits mineralization *in vivo*. (A) MicroCT-measured 3-week-old cortical bone mass (BV/TV) and mineral density (mg HA/ccm) (n=4 for $S^{+/-}$, $S^{-/-}$ and $KS^{+/-}$, 3 for $KS^{-/-}$). (B) MicroCT-measured 3-week-old trabecular bone mass and mineral density (n=5 for $S^{+/-}$, 3 for $S^{-/-}$, 4 for $KS^{+/-}$ and 3 for $KS^{-/-}$), with trabecular number, trabecular thickness and trabecular separation. (C) MicroCT-measured 5- to 8-week-old cortical bone mass and mineral density (n=9 for $S^{+/-}$, 6 for $S^{-/-}$ and 7 for $KS^{-/-}$). (D) MicroCT-measured 5- to 8-week-old trabecular bone mass and mineral density (n=10 for $S^{+/-}$ and 7 for $S^{-/-}$ and $KS^{-/-}$), with trabecular number, trabecular thickness and trabecular separation. (E,F) Histomorphometric analysis of Calcein double-labeled proximal periosteal femur of four genotypes and mineral apposition rate (MAR) quantified. Calcein was injected twice into 3-week-old (D) or 6-week-old mice (E) with a 4-day interval. Mice were harvested 2 days after the second injection (n=3 per genotype for 3 weeks, n=3-5 for 6 weeks). ****P<0.001, ***P<0.005, **P<0.01 and *P<0.05 by one-way ANOVA. Data represent mean±s.e.m.

femurs from 3-week-old mice. Sox9$^+$ cell numbers were increased in both $KS^{+/-}$ and $KS^{-/-}$ genotypes, each with a distinct distribution in the distal femur (Fig. 6E). $KS^{+/-}$ showed ectopic expansion of Sox9$^+$ cells above the growth plate, whereas $KS^{-/-}$ showed increased Sox9$^+$ chondrocytes in the proliferating and prehypertrophic zones within the growth plate (Fig. 6E). To

Development (2021) 148, dev199607. doi:10.1242/dev.199607

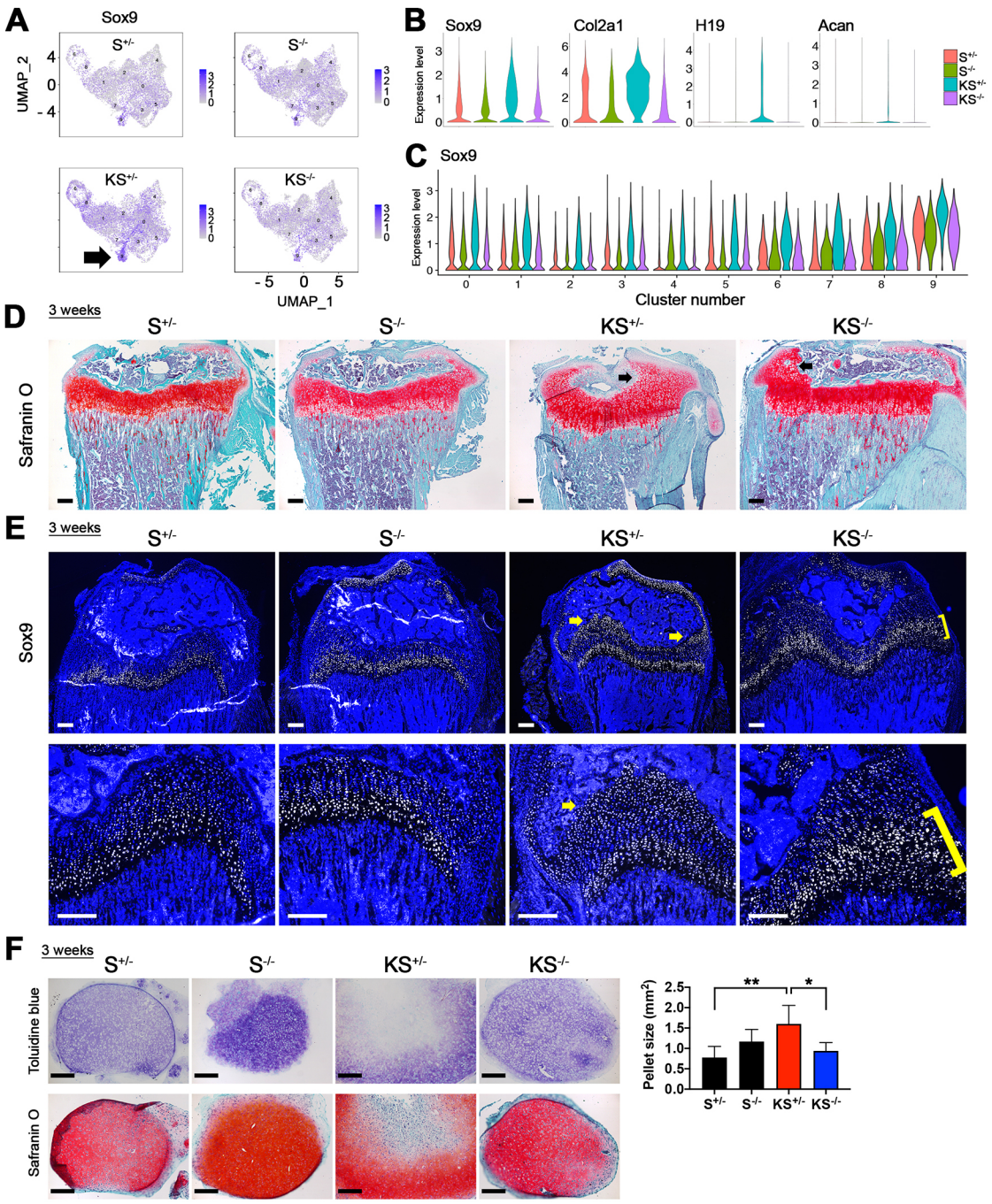

Fig. 6. PDGFRβ^{D849V} and STAT1 augment chondrogenesis. (A) Distribution of Sox9-expressing cells in UMAP between genotypes. Arrow indicates *Acan*^{high} chondrogenic precursors (cluster 9). (B) Violin plots showing expression levels of chondrogenic markers (*Sox9*, *Col2a1*, *H19* and *Acan*) in scRNA-seq across four genotypes ($S^{+/-}$, $S^{-/-}$, $KS^{+/-}$ and $KS^{-/-}$). (C) Violin plots showing expression levels of *Sox9* throughout ten clusters between four genotypes ($S^{+/-}$, $S^{-/-}$, $KS^{+/-}$ and $KS^{-/-}$). (D) Safranin-O stained 3-week-old tibias with Fast Green counterstain (n=3 for $S^{+/-}$, $S^{-/-}$ and $KS^{+/-}$ and 6 for $KS^{-/-}$). Black arrows indicate cartilage expansion. (E) Immunostaining of SOX9 in 3-week-old femurs (representative of n=3 for each genotype). Ectopic/expanded SOX9 above the growth plate indicated by yellow arrows in $KS^{+/-}$. Ectopic/expanded SOX9 within the growth plate indicated by yellow brackets in $KS^{-/-}$. Bottom panels show magnification of area of top panel. (F) Histological analysis of Toluidine Blue-stained or Safranin-O-stained chondrocyte pellets after 3 weeks of differentiation. The size of pellets was quantified with the histological sections (n=5 biological replicates per genotype). Scale bars: 200 µm. **P<0.01 and *P<0.05 by one-way ANOVA. Data represent mean±s.e.m.

examine chondrogenic differentiation *in vitro*, we isolated heterogeneous skeletal cells from 3-week-old compact bone, which includes progenitors with chondrogenic potential. We found that $KS^{+/-}$ cells dramatically increased pellet size compared with the others after 21 days in culture (Fig. 6F). Interestingly, although many $KS^{+/-}$ cells appeared to have matured into chondrocytes in matrices that were strongly positive for Toluidine Blue and Safranin-O, cells in the pellet core appeared to be undifferentiated (Fig. 6F). $KS^{+/-}$ cells often generated irregular donut-shaped or rod-shaped pellets, unlike spherical pellets formed by other genotypes. $KS^{-/-}$ cells generated chondrocyte pellets similar to controls. We further investigated transcriptional changes in $KS^{+/-}$ pellets using *in situ* hybridization. Upregulated *H19* and *Acan* mRNA expression was evident in $KS^{+/-}$ pellets (Fig. S3B),

Development (2021) 148, dev199607. doi:10.1242/dev.199607

consistent with scRNA data (Fig. 6B,C). *Col10a1* (collagen, type X, alpha 1) expression was also increased in $KS^{+/-}$ pellets (Fig. S3B). TUNEL-positive area was not increased in the majority of $KS^{+/-}$ pellets (Fig. S3C). Therefore, increased $KS^{+/-}$ chondrogenesis *in vitro* was not linked to apoptosis. Together, these findings suggest that $PDGFR\beta^{D849V}$ and STAT1 upregulate *Sox9* and enhance chondrogenesis *in vitro* and *in vivo*.

Low interferon signature in SSCs

As $KS^{+/-}$ mice showed wasting due to PDGFRβ-STAT1-mediated auto-inflammation, and $KS^{+/-}$ dermal fibroblasts intrinsically overexpress interferon-stimulated genes (ISGs) (He et al., 2017), we examined whether $KS^{+/-}$ cells from bone also exhibit an ISG signature. In $KS^{+/-}$ heterogeneous skeletal cells, a panel of ISGs was highly overexpressed (Fig. S4A). In $KS^{+/-}$ SSC-derived cells, the ISGs *Ifi27*, *Bst2*, *Isg15*, *Ifit1*, *Psmb8*, *Mx1* and *Stat1* were upregulated throughout all clusters (Fig. S4B-D). However, in SSC-derived cells the expression of ISGs was very low and was detected in few cells regardless of genotype. It has been shown that other types of stem cells are intrinsically protected from interferon responses (Burke et al., 1978; Eggenberger et al., 2019), and this may be true for SSCs.

$PDGFR\beta^{D849V}$ enhances osteoclastogenesis

PDGF signaling in osteolineage cells promotes osteoclast activity through the expression of colony stimulating factor 1 (*Csf1*) and receptor activator of nuclear factor kappa-B ligand (*Rankl*; *Tnfsf11*) (Brun et al., 2020; Chen et al., 2015). From our mutant scRNA-seq data (Table S3), we found changes in several genes that are linked to osteoclastogenesis (Table S10), although we did not observe increased *Csf1* or *Rankl*. Instead, positive regulators of osteoclasts such as *Igfbp5* (in $KS^{+/-}$) and *Igf1* (in both $KS^{+/-}$ and $KS^{-/-}$) were upregulated. Negative regulators were downregulated including clusterin (*Clu*), cystatin C (*Cst3*), *Cxcl15* and fibromodulin (*Fmod*) in $KS^{+/-}$, and *Serpinf1* in both $KS^{+/-}$ and $KS^{-/-}$. These changes suggest enhanced osteoclastogenesis in the context of $PDGFR\beta^{D849V}$. To evaluate osteoclasts *in vivo*, we performed tartrate-resistant acid phosphate (TRAP) staining. The TRAP-positive area covering trabecular bone surface approximately doubled in both $KS^{+/-}$ and $KS^{-/-}$ mutant femurs at 3 weeks of age (Fig. S5A). These findings suggest that $PDGFR\beta^{D849V}$ promotes osteoclast activity through multiple mechanisms. $PDGFR\beta^{D849V}$-mediated osteoclastogenesis may be also dependent on RANKL, as many of the differentially expressed osteoclast regulators work through RANKL (Kram et al., 2017; Strålberg et al., 2013; Wang et al., 2006) (Table S10).

$PDGFR\beta^{D849V}$ activates STAT5 and increases IGF1 expression

Although both $KS^{+/-}$ and $KS^{-/-}$ mutants showed defective mineralization, only $KS^{-/-}$ showed overgrowth *in vivo*. From scRNA-seq, we found that *Igf1* and *Socs2* were highly upregulated in $KS^{-/-}$ SSC-derived cells and were upregulated to a lesser amount in $KS^{+/-}$ cells, compared with controls (Fig. 7A). Increased *Igf1* and

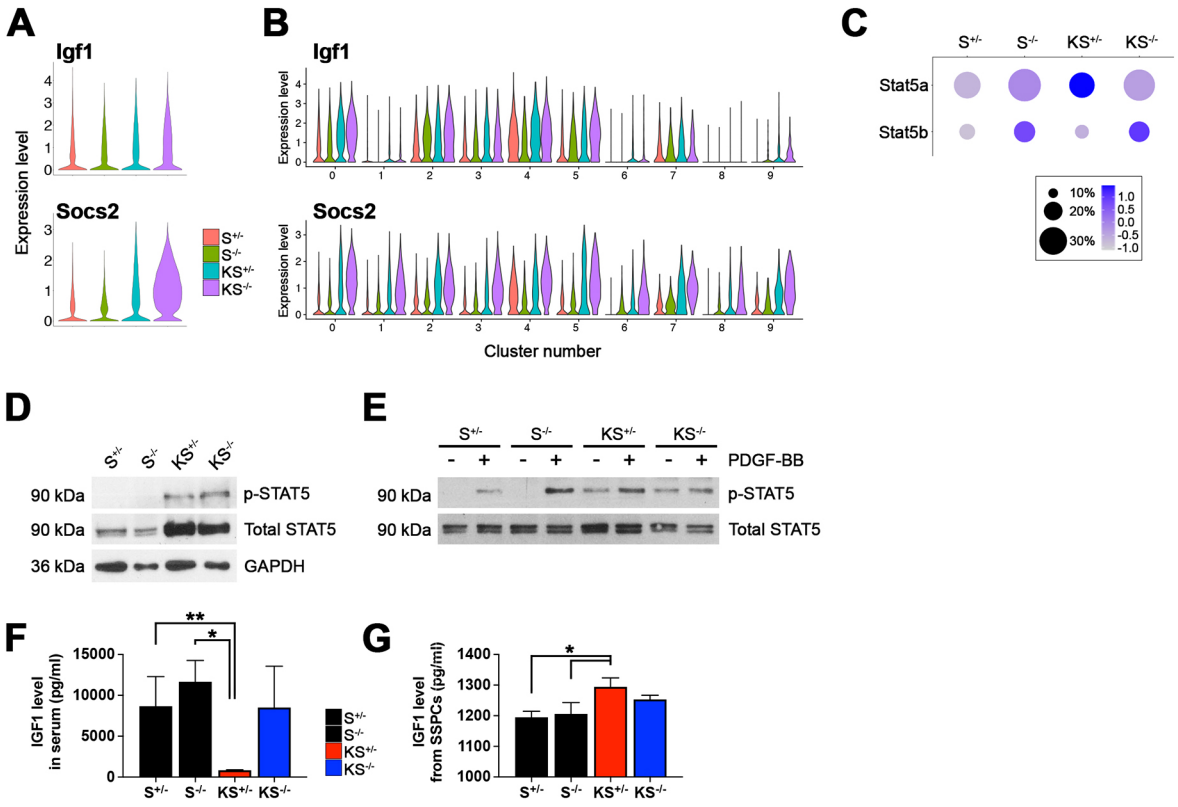

Fig. 7. $PDGFR\beta^{D849V}$ activates STAT5 and increases IGF1 expression. (A) Violin plots showing expression levels of *Igf1* and *Socs2* in scRNA-seq across four genotypes ($S^{+/-}$, $S^{-/-}$, $KS^{+/-}$ and $KS^{-/-}$). (B) Violin plots showing expression levels of *Igf1* and *Socs2* throughout ten clusters across four genotypes ($S^{+/-}$, $S^{-/-}$, $KS^{+/-}$ and $KS^{-/-}$). (C) Expression levels and percent expression of *Stat5a* and *Stat5b* in all clusters of scRNA-seq. (D) Phosphorylated STAT5 (pY694) and total STAT5 in SSC-derived cells after overnight serum-starvation, representative of two biological replicates. (E) Phosphorylated STAT5 (pY694) and total STAT5 in skeletal cells after overnight serum-starvation PDGF-BB, representative of three biological replicates. (F) IGF1 levels in serum collected from 3-week-old mice (n=5 for $S^{+/-}$, $S^{-/-}$ and $KS^{-/-}$ and 3 for $KS^{+/-}$). (G) IGF1 levels in cell culture supernatants collected from primary skeletal cells (n=3 for $S^{+/-}$, $S^{-/-}$ and $KS^{-/-}$ and 4 for $KS^{+/-}$). **P<0.01 and *P<0.05 by one-way ANOVA. Data represent mean±s.e.m.

Development (2021) 148, dev199607. doi:10.1242/dev.199607

Socs2 mRNAs were detected in most $KS^{+/-}$ and $KS^{-/-}$ clusters, from SSCs to precursors (Fig. 7B). *Igf1* and *Socs2* are direct transcriptional targets of STAT5. The STAT5-IGF1 axis is crucial for the biological effects of growth hormone receptor signaling (Chia et al., 2006; Udy et al., 1997), and SOCS2 is involved in negative feedback on STAT5 (Greenhalgh et al., 2002). It is known that PDGFRβ can phosphorylate STAT5 (Valgeirsdóttir et al., 1998), although the biological significance is unclear. Interestingly, *Stat5a* mRNA was overexpressed by $KS^{+/-}$ SSC-derived cells and *Stat5b* was overexpressed by $KS^{-/-}$ cells (Fig. 7C). However, the role of STAT5 in signaling and gene activation is mainly regulated by phosphorylation. Both $KS^{+/-}$ and $KS^{-/-}$ SSC-derived cells exhibited constitutive STAT5 phosphorylation (Fig. 7D), and STAT5 was also constitutively phosphorylated in heterogeneous skeletal cells from both mutants (Fig. 7E). The antibodies used for these western blots detect both STAT5 proteins and therefore cannot discern whether there is differential activation of the two isoforms in $KS^{+/-}$ and $KS^{-/-}$ cells. Based on these results, we suggest that the STAT5-IGF1 axis could be a key signaling pathway for PDGFRβ-mediated overgrowth. Serum IGF1 was unchanged between 3-week-old controls and $KS^{-/-}$ mice, which were not yet overgrown (Fig. 7F), but was very low in 3-week-old $KS^{+/-}$ mice, which were moribund (Fig. 7F). IGF1 levels were, however, elevated in culture medium of $KS^{+/-}$ and $KS^{-/-}$ skeletal cells (Fig. 7G). Therefore, PDGFRβ mutant skeletal lineages may promote skeletal overgrowth by increasing IGF1 levels locally, rather than systemically. We suggest that both $KS^{+/-}$ and $KS^{-/-}$ mice have potential for overgrowth due to increased signaling through the STAT5-IGF1 axis. But $KS^{+/-}$ mice do not exhibit the overgrowth phenotype because of growth-suppressive (and lethal) effects of *Stat1*-mediated autoinflammation.

DISCUSSION

Recent characterization of SSC heterogeneity and elucidation of SSC niches has greatly expanded our understanding of skeletal biology. Depletion of SSCs by conditional diphtheria toxin (DT) expression in mice has been considered one of the essential *in vivo* approaches to demonstrate the importance of SSCs in skeletal growth. For example, depletion of $PTHrP^{+}$ cells, Cxcl12-abundant reticular (CAR) cells, $Grem1^{+}$ cells, or $LepR^{+}$ cells using DT has successfully demonstrated the importance of these diverse stem cell types in chondrocyte, osteoblast and adipocyte maintenance (Mizuhashi et al., 2018; Omatsu et al., 2010; Worthley et al., 2015; Zhou et al., 2014). However, there is still much to learn in terms of signaling pathways and genes regulating SSC functions. In this study, we found that increased PDGFRβ signaling alters PαS SSC abundance and the fate of SSC-derived cells in parallel to phenotypes affecting the skeleton. Our results suggest that constitutive PDGFRβ signaling in SSCs precedes alterations in osteogenic and chondrogenic differentiation. These cell-autonomous and skeletal lineage-autonomous defects, combined with systemic effects of constitutive PDGFRβ signaling (including interferonopathy-like autoinflammation), lead to osteopenia and skeletal phenotypes that are reminiscent of humans with *PDGFRB* mutations.

Colony formation assays have historically been used to assay for the enrichment of cells with stem cell properties, but it has been challenging to identify molecular targets or cellular pathways owing to the rarity of SSCs. In our case, it was important to isolate $KS^{+/-}$ SSCs and culture them to isolate the intrinsic gene expression changes from the effects of severe autoinflammation *in vivo*. However, it is known that marker expression and biosynthetic outputs change with time in culture. Furthermore, as illustrated by our data, sorted population of stem cells becomes heterogeneous in a short time. Nevertheless, with scRNA transcriptomics of cultured SSC-derived polyclonal colonies, we were able to tentatively designate SSCs and progenitor cell types and then identify molecular alterations that were linked to phenotypes in $KS^{+/-}$ and $KS^{-/-}$ mutant mice. Thus, our work suggests the utility of using scRNA-seq even with heterogeneous cultured cells to provide new molecular understanding of diseases. Our results could potentially be refined even further by characterizing individual SSC clones through *in vivo* transplantation (Chan et al., 2015).

We found that wasting $KS^{+/-}$ mutants and overgrown $KS^{-/-}$ mutants both exhibit impaired osteogenesis *in vivo*. SSC-derived cells from both mutants decreased osteogenesis-related genes such as *Col1a1*, *Col1a2* and *Serpinf1*, and skeletal cells from both mutants showed reduced osteogenic differentiation and mineralization capacities. Human loss-of-function mutations in *COL1A1* or *COL1A2* (MIM 166200) or *SERPINF1* (MIM 172860) result in osteogenesis imperfecta, with decreased mineralization and brittle bones (Byers and Pyott, 2012). On the other hand, DEGs between $KS^{+/-}$ and $KS^{-/-}$ mutants suggest that *Stat1*-dependent mechanisms are also involved. We highlighted increased *Sox9* expression in $KS^{+/-}$ mice and SSC-derived cells as an intrinsic source of osteogenesis defects because *Sox9* overexpression in mice leads to impaired osteogenesis and dwarfism (Akiyama et al., 2004; Zhou et al., 2006). $KS^{+/-}$ osteogenesis defects *in vivo* are likely compounded by autoinflammation (Redlich and Smolen, 2012). The kidneys are crucial for maintaining healthy bones by regulating phosphorous and calcium levels in the blood. A PDGFRβ gain-of-function mutation controlled by $Foxd1Cre^{tg}$ has been shown to cause mesangioproliferative glomerulonephritis and renal fibrosis with progressive anemia in mice (Buhl et al., 2020). However, as renal phenotypes only began to appear at 6 weeks of age, renal dysfunction is unlikely to initiate skeletal phenotypes in our mice, but it may contribute to later progression in $KS^{-/-}$.

Our study suggests that $Pdgfrb^{D849V}$ signaling through STAT1 promotes *Sox9* expression and chondrocyte proliferation. We found that $KS^{+/-}$ skeletal cells formed irregularly shaped chondrocyte pellets. The non-spherical morphology may occur because of excessive cartilage matrix. For example, BM stromal cells obtained from familial osteochondritis dissecans (FOCD) patients (*ACAN* loss-of-function mutant) produce enlarged and irregularly shaped chondrocyte pellets with highly upregulated cartilage matrix proteins including collagen 11 and proteoglycans (Xu et al., 2016). We found that *Acan*, *Col2a1* and *Col11a1* were all upregulated in $KS^{+/-}$ colonies. We do not know how $Pdgfrb^{D849V}$-STAT1 regulates *Sox9*, but STAT3 has been shown to directly regulate *Sox9* in chondrogenesis (Hall et al., 2017) and STAT1 can heterodimerize with STAT3.

$Pdgfrb^{D849V}$ increases functional SSC numbers and SSC-derived cells overexpress growth signaling genes (i.e. *Igf1* and *Socs2*). STAT5 may be an important mediator of overgrowth because *Igf1* is a direct transcriptional target of STAT5, which is directly activated by PDGFRβ (Chia et al., 2006; Valgeirsdóttir et al., 1998). STAT5 is constitutively phosphorylated in $KS^{+/-}$ and $KS^{-/-}$ cells, but only $KS^{-/-}$ induces overgrowth. As discussed above, there are additional effectors in $KS^{+/-}$ to counterbalance potential overgrowth, such as STAT1-dependent autoinflammation and *Sox9* expression. Furthermore, $KS^{+/-}$ cells upregulated the expression of IGF binding proteins (IGFBP3, 6 and 7) (Tables S3,S4), potentially blocking IGF1 signals. Increased IGF1 in $KS^{-/-}$ mice appears to occur locally in skeletal cells rather than systemically, because

Development (2021) 148, dev199607. doi:10.1242/dev.199607

increased IGF1 was detected in conditioned medium from mutant cells but not in mutant mouse circulation. We do not know whether IGF1 causes overgrowth through autocrine signaling or by signaling between cell types. Tissue-specific genetic studies will be needed to investigate the involvement of a PDGFRβ-STAT5-IGF1 axis and to identify IGF1-responsive cells.

Although the D849V mutation in our study is not the same as mutations seen in Penttinen syndrome and Kosaki overgrowth syndrome, we believe our findings here are closely related to the human conditions. Osteopenia, often associated with bone fractures, is a common feature in both human diseases. For example, two Kosaki overgrowth syndrome patients developed fractured tibias and compression fractures in the spine, causing deformation of their bones (Foster et al., 2020; Minatogawa et al., 2017). Further, a Penttinen Syndrome patient exhibited osteoporosis with multiple fractures (Johnston et al., 2015). Similarly, we found osteopenia in *Pdgfrb*^{D849V} mice regardless of phenotype on the wasting-overgrowth spectrum. A better understanding of the pathogenic mechanisms of different activating PDGFRβ mutations will be obtained through future genetic models that reproduce the specific human *PDGFRB* mutations seen in Penttinen and Kosaki syndromes. The current work puts forth SSCs as a conceptual tool for considering pathological changes in the PDGFRβ mutant skeleton as resulting from altered stem cell functions.

MATERIALS AND METHODS

Animal models

Mouse strains *Pdgfrb*^{D849V} (#018435), *Sox2-Cre*^{tg} (#008454) and *Stat1*^{flox} (#012901) are available at the Jackson Laboratory. All procedures performed on mice were approved by the Institutional Animal Care and Use Committee of the Oklahoma Medical Research Foundation, USA. Mice were maintained on a mixed C57BL/6;129 genetic background with a standard mouse chow diet (5053, Purina). Mutant $KS^{+/-}$ and $KS^{-/-}$ mice were compared with age and sex-matched littermate control $S^{+/-}$ and $S^{-/-}$ mice.

Fluorescence-activated cell sorting (FACS) and CFU-F of skeletal stem cells

PαS cells were isolated by the method of Houlihan et al. (2012) with some modifications. FACS buffer was made of 1× HBSS (Gibco), 2% fetal bovine serum (FBS), 1× penicillin/streptomycin (Gibco), 1 mM ethylenediaminetetraacetic acid (EDTA, VWR) in autoclaved H_2O. Limbs of control and mutant mice at 3, 6 and 9 weeks old were dissected and soaked in 70% ethanol for 2 min, followed by careful removal of adherent muscles. BM was flushed 2-3 times with sterile PBS using a 26 G×1/2 needle and 1 ml syringe (BD Biosciences). BM-free bones were cut into small pieces with sterile scissors until bones became paste (usually 3 min for 3-week-old and 5 min for 6- to 9-week-old mice). The bone paste from each mouse was transferred to a 15 ml conical tube and enzymatically digested with 15 ml 0.2% type II collagenase (Worthington) in DMEM (Corning) for 1 h with agitation at 37°C. Digested bone paste was filtered through a 70 µm cell strainer and collected in a 50 ml conical tube on ice. Bone paste remaining on the filter was collected with 2.5 ml FACS buffer, gently tapped in a mortar with a pestle and filtered into the same 50 ml conical tube on ice. This was repeated until the total volume of filtrate reached 50 ml. After centrifugation at 280 ***g*** for 10 min at 4°C, 1 ml ice-cold sterile H_2O was used to remove red blood cells for 6 s. Then 1 ml 4% FBS in PBS and 13 ml FACS buffer were added, followed by filtering with 70 µm cell strainer into a new 50 ml tube. After centrifugation at 280 ***g*** for 5 min, re-suspended cells were incubated with fluorophore-conjugated antibodies (Table S9) on ice for 20 min in the dark. PαS cells were sorted using MoFlo XDP Cell Sorter (Beckman Coulter) or FACSAria III (BD Biosciences) by negative gating with Zombie Green™ (live/dead cell dye), CD31 (PECAM1), CD45 (PTPRC), TER119 (Ly76) and positive gating with PDGFRα and Sca1 (Fig. S1A). For colony formation assays, 2000 PαS cells or freshly isolated WBM cells were cultured in a 6-well plate with 20% FBS (mesenchymal stem cell-qualified, Gibco), 25 units/ml penicillin/streptomycin and 2 mM L-glutamine in alpha MEM (Gibco) for 2 weeks under hypoxia (5% oxygen) at 37°C. Colonies were fixed with 4% paraformaldehyde (PFA) for 15 min and stained with 0.5% Crystal Violet for quantification.

scRNA-seq and annotation

Single-cell suspensions of PαS SSC-derived colonies were harvested from CFU-F assays after culturing for 2 weeks as explained above. Trypsinized cells were filtered through a 40 µm cell strainer. A total of eight samples as four batches were generated in duplicate with one male and one female of each genotype. Each time, two samples (maximum 20,000 cells per each sample) were loaded for the 10x Genomics Chromium platform, barcoded and sequenced on the Illumina NovaSeq SP flowcell platform at a depth of 400 million reads per sample. See Table S5 for batch information and actual cell numbers sequenced and analyzed. Using the 10x Genomics Cellranger software (version 3), sequences were demultiplexed to extract cellular barcodes, cDNA inserts and unique molecular identifiers (UMIs) and the cDNA sequences were aligned to the murine mm10 genome reference to count UMIs. Quality control, data integration, clustering and gene expression analysis were performed with Seurat package V3 for R (Butler et al., 2018; Stuart et al., 2019). Cells with >8000 genes, <1500 genes or >8% of genes mapping to mitochondrial genes were removed as poor quality or doublets. Eight samples were individually normalized by using the log transformation method in Seurat. Data integration of eight samples to remove batch effect was carried out with CCA, with the top 2000 variable genes identified by FindVariableFeatures function in Seurat (Butler et al., 2018). Cells were categorized into S, G1 or G2/M phase by scoring cell cycle-associated gene expression (Kowalczyk et al., 2015). Principal component analysis (PCA) was performed by regressing out cell cycle, mitochondrial and ribosomal gene expression. The top 100 PCs were selected to perform dimensional reduction using UMAP. We determined a cluster resolution of 0.4 (total 12 clusters) using Clustree R package (graphic-based cluster resolution analyzer) (Zappia and Oshlack, 2018). Among the 12 clusters, ten were selected for analysis, because two of the clusters only included about ten cells each. A heatmap was generated with the top ten genes (Table S1) in each cluster determined by FindAllMarkers function in Seurat. For gene signature analysis, DEGs of each cluster were determined by FindMarkers function in Seurat with 0.25 log-scale fold-change threshold between two groups (i.e. genotypes). DEGs were further analyzed using DAVID to determine gene ontology and pathway identification (Huang et al., 2009). Cell types of clusters were tentatively defined with a signature gene list, gene ontology and literature as SSCs, SSPCs, chondrocyte precursors, osteoblast precursors and adipocyte precursors. To identify genotype-specific genes and clusters, we split the integrated data into four groups (individually $S^{+/-}$, $S^{-/-}$, $KS^{+/-}$ and $KS^{-/-}$). DEGs between four groups were identified using the FindMarkers function in Seurat. The scRNA data were deposited as GSE183404 in the Gene Expression Omnibus of the National Center for Biotechnology Information.

Primary skeletal cell culture and *in vitro* differentiation

Primary skeletal cells were isolated by enzymatic digestion of compact bone (Zhu et al., 2010). BM-free bones were collected as described above and were cut into small pieces (1-3 mm^3) with sterile scissors. The bone chips were transferred into a 1.6 ml microcentrifuge tube and enzymatically digested with 1.5 ml of 1 mg/ml type II collagenase (Worthington) in alpha MEM (Corning) plus 10% FBS for 1.5 h with agitation in a 37°C incubator. The bone chips were washed with 1 ml of alpha MEM three times, seeded into a 6-well plate and maintained with alpha MEM plus 10% FBS, 25 units/ml penicillin/streptomycin and 2 mM L-glutamine at 37°C. Passages 4 to 6 were used for tri-lineage differentiation assays. For osteoblast differentiation, 2×10^5 cells were seeded in a 24-well plate. On the following day, they were treated with alpha MEM supplemented with 10% FBS, 10^{-7} M dexamethasone, 10 mM β-glycerol-phosphate and 50 mM ascorbate-2-phosphate. Medium was changed three times per week for 2 weeks (early osteoblast differentiation). The samples were subjected to ALP staining with ALP buffer [100 mM Tris-HCl, 100 mM NaCl, 5 mM

Development (2021) 148, dev199607. doi:10.1242/dev.199607

$MgCl_2$, 0.05% Tween-20 in deionized water (adjusted at pH 9.5)] plus 0.02% 5-bromo-4-chloro-3-indolyl phosphate (BCIP) and 0.03% nitro blue tetrazolium (NBT). For mineralization, 1×10^5 cells were seeded in a 96-well plate and treated with the osteoblast differentiation medium mentioned above. After 4 weeks, samples were stained with 40 mM Alizarin Red. For chondrogenesis, 1×10^6 cells were pelleted in a 15 ml conical tube at 280 ***g*** for 6 min at 4°C and cultured for 3 weeks with the MesenCult™-ACF chondrogenic differentiation kit (Stemcell Technologies). Pellets were fixed with 4% PFA for 1 h, embedded in paraffin, sectioned at 8 µm and stained with 0.05% Toluidine Blue or 1% Safranin-O.

PαS SSC-derived polyclonal colony differentiation

For osteogenesis using PαS-derived colonies, colonies cultured for 2 weeks under hypoxia were further treated with the osteogenesis inducers as described above for an additional 2 weeks under normoxia and stained with ALP (Fast Green as a counterstain). For adipogenesis, 2-week-cultured colonies were treated with alpha MEM supplemented with 10% FBS, 10^{-6} M dexamethasone, 250 µM IBMX, 10 µg/ml insulin and 5 nM rosiglitazone for 2 days. Colonies were maintained with alpha MEM plus 10% FBS and 10 ng/ml insulin for an additional 8 days by changing three times in a week. Adipocytes were stained with Oil-O-Red stain (Fast Green as a counterstain).

Enzyme-linked immunosorbent assay (ELISA)

IGF1 levels were measured in serum and skeletal cell culture supernatant using ELISA (Sigma-Aldrich, RAB-0229) according to the manufacturer's protocol. Blood was collected from four genotypes at 3 weeks old, incubated at room temperature for 30 min, and centrifuged at 1000 rpm (94 ***g***) for 10 min at 4°C. Clear supernatant was stored at −20°C until used. Primary skeletal cells (passages 4-5) isolated from compact bone of four genotypes at 3 weeks were cultured in a 24-well plate until confluent. After washing three times with sterile PBS, 500 µl serum-free fresh alpha MEM was replaced and cultured for 72 h. Cell culture supernatant was filtered through a 20 µm cell-strainer and stored at −20°C until used. Both serum and cell culture supernatant were diluted to 1:100 for ELISA.

Western blotting

For PαS SSC-derived cells, plates of colonies were starved in medium containing 0.2% FBS for 24 h. For skeletal cells, cells were starved in medium containing 0.1% FBS for 24 h and treated with 10 ng/ml PDGF-BB (R&D Systems) for 10-15 min. Cells were then lysed in RIPA buffer [50 mM Tris (pH 7.4), 1% NP-40, 0.25% sodium deoxycholate, 150 mM NaCl, 0.1% sodium dodecyl sulfate] with 1 mM NaF, Na_3VO_4, PMSF and 1× protease inhibitor cocktail (Complete, Roche). Pierce BCA assay was used to determine protein concentration. Aliquots of 5-10 µg of protein were separated by SDS-PAGE (using parallel gels for proteins of similar size), transferred to nitrocellulose membranes, blocked with 5% BSA and incubated with primary antibodies (Table S9) overnight at 4°C. Membranes were probed with horseradish peroxidase (HRP)-conjugated secondary antibodies at 1:5000 (Jackson ImmunoResearch) in 5% milk. Pierce ECL Western blotting substrate (Thermo Fisher Scientific) and autoradiography film (Santa Cruz Biotechnology) were used to develop blots.

RNA isolation and qRT-PCR

Total RNA was isolated from cultured primary skeletal cells enriched from compact bones using Trizol (Thermo Fisher Scientific). cDNA reverse transcription was performed with Superscript III RT (Invitrogen) and random primers. Quantitative PCR was performed using a Bio-Rad iCycler with iQ TM SYBR green master mix and designated primers (Table S8).

Tissue histology and immunostaining

Tissue was fixed overnight in 10% neutral buffered formalin (NBF; Sigma-Aldrich) or 4% PFA (Electron Microscopy). Bones were decalcified in 0.5 M EDTA solution (pH 7.4) for 2 weeks at room temperature. For cartilage staining, fixed tissues were embedded in paraffin and sectioned at 6 µm thickness followed by Hematoxylin and Eosin (H&E) or Safranin-O staining (Fast Green and Hematoxylin as counterstain). For TRAP staining, fixed tissues were decalcified in 0.5 M EDTA solution at 4°C, dehydrated in 20% sucrose in PBS and cryosectioned at 8-10 µm thickness followed by Naphthol AS-BI phosphoric acid and diazotized Fast Garnet GBC stains (Fast Green as counterstain) (Sigma-Aldrich, 387A). For immunostaining, PFA-fixed tissues were cryosectioned at 8-12 µm. Slides were stained with primary antibody (Table S9) and conjugated secondary antibody (Jackson ImmunoResearch), with DAPI (Sigma-Aldrich) as a nuclear stain. For TUNEL staining, pellets were cryosectioned at 6 µm, permeabilized with 0.1% Triton X-100 and 0.1% sodium citrate for 2 min on ice, incubated with 50 µl TUNEL reaction mixture (5 µl enzyme solution and 45 µl label solution) (Roche) for 1 h at 37°C, and stained with DAPI. Imaging was performed using a Nikon Eclipse 80i microscope with a digital camera.

In situ hybridization

Probes were generated from template sequences (Table S7). Chondrocyte pellets were fixed with 4% PFA for 1-3 h, dehydrated in 20% sucrose in PBS and cryosectioned at 6 µm thickness. Antisense digoxigenin (Dig)-labeled RNA probes were synthesized using Dig RNA labeling mix (Roche) from cDNA template sequences. Hybridized probes were detected with anti-Dig Fab fragments (Roche) and developed with NBT/BCIP.

Bone formation rate and microcomputed tomography

To measure the MAR of bone formation, double Calcein stain was performed. Calcein (10 mg/kg, Sigma-Aldrich) in 0.9% NaCl and 2% $NaHCO_3$ was intraperitoneally injected in 3- or 6-week-old mice with a 4-day interval. Mice were harvested 2 days after the second injection. Paraffin sectioning was performed following the method of Porter et al. (2017): femurs were harvested with adherent muscles and fixed with formalin for 2 days, then cleared with 10% KOH for 96 h. The tissues were embedded in paraffin and sectioned at 6 µm thickness, pre-soaking the paraffin blocks in 1% KOH immediately before sectioning. Imaging was performed using a FITC filter with a Nikon Eclipse 80i microscope with a digital camera. To get clear fluorochrome images with minimal background autofluorescence, we adjusted 'Shadows' in the levels histogram in the software (NIS Elements D 3.2) using the same setting across samples. For microCT, tibias were harvested and stored in 70% ethanol at 4°C, then analyzed to measure bone volume (mm^3), total volume (mm^3), mean/density (mg HA/ccm), trabecular numbers (1/mm), trabecular thickness (mm) and trabecular separation (mm) with a VivaCT 40 microCT (Scanco Medical) at an X-ray tube voltage of 70 kVp and an X-ray current of 114 µA for 2- to 3-week-old bones, or 55 kVp and 85 µA for older bones.

Image quantification and statistics analysis

The size of CFU-F and chondrocyte pellets, the distance between double Calcein stain, and coverage area for TRAP, ALP and AR were quantified with ImageJ software (National Institutes of Health). The Set Scale function was used to convert units from pixels to mm or µm with known scale of images. Regions of interest (ROIs) were selected using the oval or polygon selection tool to measure the area of CFU-F and pellet images. The straight tool was used to measure the distance between double Calcein stain. Coverage area were calculated by 8-bit gray scale conversion and thresholding to measure area fraction within ROIs. Statistical calculations were performed using GraphPad Prism 9 with one-way or two-way ANOVA or unpaired, two-tailed *t*-test. Data are represented as mean±s.e.m.

Acknowledgements

We thank Jacquelyn C. Herron, Shouan Zhu, Mary Beth Humphrey, Timothy M. Griffin and members of the Olson lab for their assistance and helpful discussion. We also thank the Microscopy Core and Mouse Phenotyping Core Facilities (associated with P30-GM114731) of the Oklahoma Medical Research Foundation Centers of Biomedical Research Excellence.

Competing interests

The authors declare no competing or financial interests.

Author contributions

Conceptualization: H.R.K., L.E.O.; Investigation: H.R.K., J.H.K., J.P.W.; Writing - original draft: H.R.K.; Writing - review & editing: H.R.K., J.P.W., L.E.O.; Visualization: H.R.K.; Supervision: L.E.O.; Funding acquisition: H.R.K., L.E.O.

Funding
H.R.K. was supported by grant F32-HL142222 from the National Institutes of Health/National Heart, Lung, and Blood Institute. This work was supported by US National Institutes of Health grants R01-AR073828 and R01-AR070235 (L.E.O.), grants from the Oklahoma Center for Adult Stem Cell Research (a program of Tobacco Settlement Endowment Trust), and support from the Presbyterian Health Foundation. Deposited in PMC for release after 12 months.

Data availability
scRNA data have been deposited in GEO under accession number GSE183404.

Peer review history
The peer review history is available online at https://journals.biologists.com/dev/article-lookup/doi/10.1242/dev.199607.

References

Akiyama, H., Chaboissier, M. C., Martin, J. F., Schedl, A. and de Crombrugghe, B. (2002). The transcription factor Sox9 has essential roles in successive steps of the chondrocyte differentiation pathway and is required for expression of Sox5 and Sox6. *Genes Dev.* **16**, 2813-2828. doi:10.1101/gad.1017802

Akiyama, H., Lyons, J. P., Mori-Akiyama, Y., Yang, X., Zhang, R., Zhang, Z., Deng, J. M., Taketo, M. M., Nakamura, T., Behringer, R. R. et al. (2004). Interactions between Sox9 and beta-catenin control chondrocyte differentiation. *Genes Dev.* **18**, 1072-1087. doi:10.1101/gad.1171104

Ambrosi, T. H., Longaker, M. T. and Chan, C. K. F. (2019). A revised perspective of skeletal stem cell biology. *Front. Cell Dev. Biol.* **7**, 189. doi:10.3389/fcell.2019.00189

Andrae, J., Gallini, R. and Betsholtz, C. (2008). Role of platelet-derived growth factors in physiology and medicine. *Genes Dev.* **22**, 1276-1312. doi:10.1101/gad.1653708

Bell, D. M., Leung, K. K. H., Wheatley, S. C., Ng, L. J., Zhou, S., Ling, K. W., Sham, M. H., Koopman, P., Tam, P. P. L. and Cheah, K. S. E. (1997). SOX9 directly regulates the type-II collagen gene. *Nat. Genet.* **16**, 174-178. doi:10.1038/ng0697-174

Bianco, P. and Robey, P. G. (2015). Skeletal stem cells. *Development* **142**, 1023-1027. doi:10.1242/dev.102210

Bohm, A. M., Dirckx, N., Tower, R. J., Peredo, N., Vanuytven, S., Theunis, K., Nefyodova, E., Cardoen, R., Lindner, V., Voet, T. et al. (2019). Activation of skeletal stem and progenitor cells for bone regeneration is driven by PDGFRbeta signaling. *Dev. Cell* **51**, 236-254.e212. doi:10.1016/j.devcel.2019.08.013

Bredrup, C., Stokowy, T., McGaughran, J., Lee, S., Sapkota, D., Cristea, I., Xu, L., Tveit, K. S., Høvding, G., Steen, V. M. et al. (2019). A tyrosine kinase-activating variant Asn666Ser in PDGFRB causes a progeria-like condition in the severe end of Penttinen syndrome. *Eur. J. Hum. Genet.* **27**, 574-581. doi:10.1038/s41431-018-0323-z

Brun, J., Andreasen, C. M., Ejersted, C., Andersen, T. L., Caverzasio, J. and Thouverey, C. (2020). PDGF receptor signaling in osteoblast lineage cells controls bone resorption through upregulation of Csf1 expression. *J. Bone Miner. Res.* **35**, 2458-2469. doi:10.1002/jbmr.4150

Buhl, E. M., Djudjaj, S., Klinkhammer, B. M., Ermert, K., Puelles, V. G., Lindenmeyer, M. T., Cohen, C. D., He, C., Borkham-Kamphorst, E., Weiskirchen, R. et al. (2020). Dysregulated mesenchymal PDGFR-beta drives kidney fibrosis. *EMBO Mol. Med.* **12**, e11021. doi:10.15252/emmm.201911021

Burke, D. C., Graham, C. F. and Lehman, J. M. (1978). Appearance of interferon inducibility and sensitivity during differentiation of murine teratocarcinoma cells in vitro. *Cell* **13**, 243-248. doi:10.1016/0092-8674(78)90193-9

Butler, A., Hoffman, P., Smibert, P., Papalexi, E. and Satija, R. (2018). Integrating single-cell transcriptomic data across different conditions, technologies, and species. *Nat. Biotechnol.* **36**, 411-420. doi:10.1038/nbt.4096

Byers, P. H. and Pyott, S. M. (2012). Recessively inherited forms of osteogenesis imperfecta. *Annu. Rev. Genet.* **46**, 475-497. doi:10.1146/annurev-genet-110711-155608

Chan, C. K. F., Seo, E. Y., Chen, J. Y., Lo, D., McArdle, A., Sinha, R., Tevlin, R., Seita, J., Vincent-Tompkins, J., Wearda, T. et al. (2015). Identification and specification of the mouse skeletal stem cell. *Cell* **160**, 285-298. doi:10.1016/j.cell.2014.12.002

Chen, W., Baylink, D. J., Brier-Jones, J., Neises, A., Kiroyan, J. B., Rundle, C. H., Lau, K.-H. W. and Zhang, X.-B. (2015). PDGFB-based stem cell gene therapy increases bone strength in the mouse. *Proc. Natl. Acad. Sci. USA* **112**, E3893-E3900. doi:10.1073/pnas.1501759112

Chia, D. J., Ono, M., Woelfle, J., Schlesinger-Massart, M., Jiang, H. and Rotwein, P. (2006). Characterization of distinct Stat5b binding sites that mediate growth hormone-stimulated IGF-I gene transcription. *J. Biol. Chem.* **281**, 3190-3197. doi:10.1074/jbc.M510204200

Chou, D. B., Sworder, B., Bouladoux, N., Roy, C. N., Uchida, A. M., Grigg, M., Robey, P. G. and Belkaid, Y. (2012). Stromal-derived IL-6 alters the balance of myeloerythroid progenitors during Toxoplasma gondii infection. *J. Leukoc. Biol.* **92**, 123-131. doi:10.1189/jlb.1011527

Debnath, S., Yallowitz, A. R., McCormick, J., Lalani, S., Zhang, T., Xu, R., Li, N., Liu, Y., Yang, Y. S., Eiseman, M. et al. (2018). Discovery of a periosteal stem cell mediating intramembranous bone formation. *Nature* **562**, 133-139. doi:10.1038/s41586-018-0554-8

Demoulin, J.-B. and Essaghir, A. (2014). PDGF receptor signaling networks in normal and cancer cells. *Cytokine Growth Factor. Rev.* **25**, 273-283. doi:10.1016/j.cytogfr.2014.03.003

Dudek, K. A., Lafont, J. E., Martinez-Sanchez, A. and Murphy, C. L. (2010). Type II collagen expression is regulated by tissue-specific miR-675 in human articular chondrocytes. *J. Biol. Chem.* **285**, 24381-24387. doi:10.1074/jbc.M110.111328

Eggenberger, J., Blanco-Melo, D., Panis, M., Brennand, K. J. and tenOever, B. R. (2019). Type I interferon response impairs differentiation potential of pluripotent stem cells. *Proc. Natl. Acad. Sci. USA* **116**, 1384-1393. doi:10.1073/pnas.1812449116

Foster, A., Chalot, B., Antoniadi, T., Schaefer, E., Keelagher, R., Ryan, G., Thomas, Q., Philippe, C., Bruel, A.-L., Sorlin, A. et al. (2020). Kosaki overgrowth syndrome: a novel pathogenic variant in PDGFRB and expansion of the phenotype including cerebrovascular complications. *Clin. Genet.* **98**, 19-31. doi:10.1111/cge.13752

Greenhalgh, C. J., Bertolino, P., Asa, S. L., Metcalf, D., Corbin, J. E., Adams, T. E., Davey, H. W., Nicola, N. A., Hilton, D. J. and Alexander, W. S. (2002). Growth enhancement in suppressor of cytokine signaling 2 (SOCS-2)-deficient mice is dependent on signal transducer and activator of transcription 5b (STAT5b). *Mol. Endocrinol.* **16**, 1394-1406. doi:10.1210/mend.16.6.0845

Guérit, E., Arts, F., Dachy, G., Boulouadnine, B. and Demoulin, J.-B. (2021). PDGF receptor mutations in human diseases. *Cell. Mol. Life Sci.* **78**, 3867-3881. doi:10.1007/s00018-020-03753-y

Hall, M. D., Murray, C. A., Valdez, M. J. and Perantoni, A. O. (2017). Mesoderm-specific Stat3 deletion affects expression of Sox9 yielding Sox9-dependent phenotypes. *PLoS Genet.* **13**, e1006610. doi:10.1371/journal.pgen.1006610

He, C. Y., Medley, S. C., Kim, J., Sun, C. Y., Kwon, H. R., Sakashita, H., Pincu, Y., Yao, L. B., Eppard, D., Dai, B. J. et al. (2017). STAT1 modulates tissue wasting or overgrowth downstream from PDGFRβ. *Gene Dev.* **31**, 1666-1678. doi:10.1101/gad.300384.117

Heldin, C.-H. and Westermark, B. (1999). Mechanism of action and in vivo role of platelet-derived growth factor. *Physiol. Rev.* **79**, 1283-1316. doi:10.1152/physrev.1999.79.4.1283

Hoch, R. V. and Soriano, P. (2003). Roles of PDGF in animal development. *Development* **130**, 4769-4784. doi:10.1242/dev.00721

Houlihan, D. D., Mabuchi, Y., Morikawa, S., Niibe, K., Araki, D., Suzuki, S., Okano, H. and Matsuzaki, Y. (2012). Isolation of mouse mesenchymal stem cells on the basis of expression of Sca-1 and PDGFR-α. *Nat. Protoc.* **7**, 2103-2111. doi:10.1038/nprot.2012.125

Huang, D. W., Sherman, B. T. and Lempicki, R. A. (2009). Systematic and integrative analysis of large gene lists using DAVID bioinformatics resources. *Nat. Protoc.* **4**, 44-57. doi:10.1038/nprot.2008.211

Johnston, J. J., Sanchez-Contreras, M. Y., Keppler-Noreuil, K. M., Sapp, J., Crenshaw, M., Finch, N. C. A., Cormier-Daire, V., Rademakers, R., Sybert, V. P. and Biesecker, L. G. (2015). A point mutation in PDGFRB causes autosomal-dominant Penttinen syndrome. *Am. J. Hum. Genet.* **97**, 465-474. doi:10.1016/j.ajhg.2015.07.009

Klinkhammer, B. M., Floege, J. and Boor, P. (2018). PDGF in organ fibrosis. *Mol. Aspects Med.* **62**, 44-62. doi:10.1016/j.mam.2017.11.008

Kowalczyk, M. S., Tirosh, I., Heckl, D., Rao, T. N., Dixit, A., Haas, B. J., Schneider, R. K., Wagers, A. J., Ebert, B. L. and Regev, A. (2015). Single-cell RNA-seq reveals changes in cell cycle and differentiation programs upon aging of hematopoietic stem cells. *Genome Res.* **25**, 1860-1872. doi:10.1101/gr.192237.115

Kram, V., Kilts, T. M., Bhattacharyya, N., Li, L. and Young, M. F. (2017). Small leucine rich proteoglycans, a novel link to osteoclastogenesis. *Sci. Rep.* **7**, 12627. doi:10.1038/s41598-017-12651-6

Lemmon, M. A. and Schlessinger, J. (2010). Cell signaling by receptor tyrosine kinases. *Cell* **141**, 1117-1134. doi:10.1016/j.cell.2010.06.011

Méndez-Ferrer, S., Michurina, T. V., Ferraro, F., Mazloom, A. R., Macarthur, B. D., Lira, S. A., Scadden, D. T., Ma'ayan, A., Enikolopov, G. N. and Frenette, P. S. (2010). Mesenchymal and haematopoietic stem cells form a unique bone marrow niche. *Nature* **466**, 829-834. doi:10.1038/nature09262

Meraz, M. A., White, J. M., Sheehan, K. C. F., Bach, E. A., Rodig, S. J., Dighe, A. S., Kaplan, D. H., Riley, J. K., Greenlund, A. C., Campbell, D. et al. (1996). Targeted disruption of the Stat1 gene in mice reveals unexpected physiologic specificity in the JAK-STAT signaling pathway. *Cell* **84**, 431-442. doi:10.1016/S0092-8674(00)81288-X

Minatogawa, M., Takenouchi, T., Tsuyusaki, Y., Iwasaki, F., Uehara, T., Kurosawa, K., Kosaki, K. and Curry, C. J. (2017). Expansion of the phenotype of Kosaki overgrowth syndrome. *Am. J. Med. Genet. A* **173**, 2422-2427. doi:10.1002/ajmg.a.38310

Mizuhashi, K., Ono, W., Matsushita, Y., Sakagami, N., Takahashi, A., Saunders, T. L., Nagasawa, T., Kronenberg, H. M. and Ono, N. (2018).

Resting zone of the growth plate houses a unique class of skeletal stem cells. *Nature* **563**, 254-258. doi:10.1038/s41586-018-0662-5

Morikawa, S., Mabuchi, Y., Kubota, Y., Nagai, Y., Niibe, K., Hiratsu, E., Suzuki, S., Miyauchi-Hara, C., Nagoshi, N., Sunabori, T. et al. (2009). Prospective identification, isolation, and systemic transplantation of multipotent mesenchymal stem cells in murine bone marrow. *J. Exp. Med.* **206**, 2483-2496. doi:10.1084/jem.20091046

Newton, P. T., Li, L., Zhou, B., Schweingruber, C., Hovorakova, M., Xie, M., Sun, X., Sandhow, L., Artemov, A. V., Ivashkin, E. et al. (2019). A radical switch in clonality reveals a stem cell niche in the epiphyseal growth plate. *Nature* **567**, 234-238. doi:10.1038/s41586-019-0989-6

Olson, L. E. and Soriano, P. (2011). PDGFRbeta signaling regulates mural cell plasticity and inhibits fat development. *Dev. Cell* **20**, 815-826. doi:10.1016/j.devcel.2011.04.019

Omatsu, Y., Sugiyama, T., Kohara, H., Kondoh, G., Fujii, N., Kohno, K. and Nagasawa, T. (2010). The essential functions of adipo-osteogenic progenitors as the hematopoietic stem and progenitor cell niche. *Immunity* **33**, 387-399. doi:10.1016/j.immuni.2010.08.017

Ortinau, L. C., Wang, H., Lei, K., Deveza, L., Jeong, Y., Hara, Y., Grafe, I., Rosenfeld, S. B., Lee, D., Lee, B. et al. (2019). Identification of Functionally Distinct Mx1+alphaSMA+ Periosteal Skeletal Stem Cells. *Cell Stem Cell* **25**, 784-796.e785. doi:10.1016/j.stem.2019.11.003

Porter, A., Irwin, R., Miller, J., Horan, D. J., Robling, A. G. and McCabe, L. R. (2017). Quick and inexpensive paraffin-embedding method for dynamic bone formation analyses. *Sci. Rep.* **7**, 42505. doi:10.1038/srep42505

Redlich, K. and Smolen, J. S. (2012). Inflammatory bone loss: pathogenesis and therapeutic intervention. *Nat. Rev. Drug Discov.* **11**, 234-250. doi:10.1038/nrd3669

Sacchetti, B., Funari, A., Michienzi, S., Di Cesare, S., Piersanti, S., Saggio, I., Tagliafico, E., Ferrari, S., Robey, P. G., Riminucci, M. et al. (2007). Self-renewing osteoprogenitors in bone marrow sinusoids can organize a hematopoietic microenvironment. *Cell* **131**, 324-336. doi:10.1016/j.cell.2007.08.025

Serowoky, M. A., Arata, C. E., Crump, J. G. and Mariani, F. V. (2020). Skeletal stem cells: insights into maintaining and regenerating the skeleton. *Development* **147**, dev179325. doi:10.1242/dev.179325

Shi, Y., He, G., Lee, W.-C., McKenzie, J. A., Silva, M. J. and Long, F. (2017). Gli1 identifies osteogenic progenitors for bone formation and fracture repair. *Nat. Commun.* **8**, 2043. doi:10.1038/s41467-017-02171-2

Soriano, P. (1994). Abnormal kidney development and hematological disorders in PDGF beta-receptor mutant mice. *Genes Dev.* **8**, 1888-1896. doi:10.1101/gad.8.16.1888

Strålberg, F., Henning, P., Gjertsson, I., Kindlund, B., Souza, P. P. C., Persson, E., Abrahamson, M., Kasprzykowski, F., Grubb, A. and Lerner, U. H. (2013). Cysteine proteinase inhibitors regulate human and mouse osteoclastogenesis by interfering with RANK signaling. *FASEB J.* **27**, 2687-2701. doi:10.1096/fj.12-211748

Stuart, T., Butler, A., Hoffman, P., Hafemeister, C., Papalexi, E., Mauck, W. M., III, Hao, Y., Stoeckius, M., Smibert, P. and Satija, R. (2019). Comprehensive integration of single-cell data. *Cell* **177**, 1888-1902.e1821. doi:10.1016/j.cell.2019.05.031

Takenouchi, T., Yamaguchi, Y., Tanikawa, A., Kosaki, R., Okano, H. and Kosaki, K. (2015). Novel overgrowth syndrome phenotype due to recurrent de novo PDGFRB mutation. *J. Pediatr.* **166**, 483-486. doi:10.1016/j.jpeds.2014.10.015

Tallquist, M. and Kazlauskas, A. (2004). PDGF signaling in cells and mice. *Cytokine Growth Factor. Rev.* **15**, 205-213. doi:10.1016/j.cytogfr.2004.03.003

Udy, G. B., Towers, R. P., Snell, R. G., Wilkins, R. J., Park, S.-H., Ram, P. A., Waxman, D. J. and Davey, H. W. (1997). Requirement of STAT5b for sexual dimorphism of body growth rates and liver gene expression. *Proc. Natl. Acad. Sci. USA* **94**, 7239-7244. doi:10.1073/pnas.94.14.7239

Valgeirsdóttir, S., Paukku, K., Silvennoinen, O., Heldin, C.-H. and Claesson-Welsh, L. (1998). Activation of Stat5 by platelet-derived growth factor (PDGF) is dependent on phosphorylation sites in PDGF beta-receptor juxtamembrane and kinase insert domains. *Oncogene* **16**, 505-515. doi:10.1038/sj.onc.1201555

Wang, Y., Nishida, S., Elalieh, H. Z., Long, R. K., Halloran, B. P. and Bikle, D. D. (2006). Role of IGF-I signaling in regulating osteoclastogenesis. *J. Bone Miner. Res.* **21**, 1350-1358. doi:10.1359/jbmr.060610

Worthley, D. L., Churchill, M., Compton, J. T., Tailor, Y., Rao, M., Si, Y., Levin, D., Schwartz, M. G., Uygur, A., Hayakawa, Y. et al. (2015). Gremlin 1 identifies a skeletal stem cell with bone, cartilage, and reticular stromal potential. *Cell* **160**, 269-284. doi:10.1016/j.cell.2014.11.042

Xu, M., Stattin, E.-L., Shaw, G., Heinegård, D., Sullivan, G., Wilmut, I., Colman, A., Onnerfjord, P., Khabut, A., Aspberg, A. et al. (2016). Chondrocytes derived from mesenchymal stromal cells and induced pluripotent cells of patients with familial osteochondritis dissecans exhibit an endoplasmic reticulum stress response and defective matrix assembly. *Stem Cells Transl. Med.* **5**, 1171-1181. doi:10.5966/sctm.2015-0384

Yang, W., Wang, J., Moore, D. C., Liang, H., Dooner, M., Wu, Q., Terek, R., Chen, Q., Ehrlich, M. G., Quesenberry, P. J. et al. (2013). Ptpn11 deletion in a novel progenitor causes metachondromatosis by inducing hedgehog signalling. *Nature* **499**, 491-495. doi:10.1038/nature12396

Zappia, L. and Oshlack, A. (2018). Clustering trees: a visualization for evaluating clusterings at multiple resolutions. *Gigascience* **7**, giy083. doi:10.1093/gigascience/giy083

Zhao, H., Feng, J., Ho, T.-V., Grimes, W., Urata, M. and Chai, Y. (2015). The suture provides a niche for mesenchymal stem cells of craniofacial bones. *Nat. Cell Biol.* **17**, 386-396. doi:10.1038/ncb3139

Zhou, G., Zheng, Q., Engin, F., Munivez, E., Chen, Y., Sebald, E., Krakow, D. and Lee, B. (2006). Dominance of SOX9 function over RUNX2 during skeletogenesis. *Proc. Natl. Acad. Sci. USA* **103**, 19004-19009. doi:10.1073/pnas.0605170103

Zhou, B. O., Yue, R., Murphy, M. M., Peyer, J. G. and Morrison, S. J. (2014). Leptin-receptor-expressing mesenchymal stromal cells represent the main source of bone formed by adult bone marrow. *Cell Stem Cell* **15**, 154-168. doi:10.1016/j.stem.2014.06.008

Zhu, H., Guo, Z.-K., Jiang, X.-X., Li, H., Wang, X.-Y., Yao, H.-Y., Zhang, Y. and Mao, N. (2010). A protocol for isolation and culture of mesenchymal stem cells from mouse compact bone. *Nat. Protoc.* **5**, 550-560. doi:10.1038/nprot.2009.238